underestimate the CO in general.[17,18] Our unpublished analysis demonstrated that the bias ± limits of agreement of the current version of the NICO monitor was −0.18 ± 1.70 L/min against standard ICO. However, when CO values derived from ICO were used in the same calculation, the limits of agreement remained large. Thus, using a presumably more accurate and instantaneous CO data from ICO failed to increase the accuracy of the estimation of SvO_2. These findings suggest that the inaccuracy of CO data from the NICO monitor cannot fully account for the variability between the estimated and measured SvO_2. Furthermore, the temporal delay of NICO-derived CO after hemodynamic change may also contribute to the wide variability. Although the response time of the NICO monitor has not yet been determined, SvO_2 changes are generally believed to change more rapidly than continuous CO and NICO. Alternatively, the response of SvO_2 to the actual hemodynamic change may be delayed, because the physiological process, such as increasing oxygen extraction in tissues, is involved in this process. These possibilities remain to be evaluated. Second, several assumptions used in this study may contribute to the observed variability. For example, Hb concentration may be a source of error, because it is only determined intermittently and the interpolated value between these measurement was used in this study. However, bias ± limits of agreement of paired measurements was not significantly improved when the Hb was measured (data not shown). Similarly, using SaO_2 data obtained from blood gas analysis did not improve the accuracy either. Therefore, the Hb concentration or Spo_2 may not be a major source of error. Recently, a device that continuously and percutaneously measures Hb has become available. Thus, with the advance of technology, this issue may be resolved in the future. Using VCO_2 to estimate VO_2 is another potential source of error in this estimation. We used a fixed 0.85 value of the VCO_2/VO_2 ratio to convert VCO_2 to VO_2 throughout this study to make monitoring settings as simple as possible. Although it is intuitively obvious that the ratio may significantly vary in anesthetized patients and critically ill patients, this variability may primarily contribute to the large limits of agreement found in this study. Although measuring VO_2 instead of VCO_2 should improve the accuracy, the precise and continuous determination of VO_2 requires specialized equipment and may substantially compromise the applicability of this method.

It is debatable whether the estimated value of SvO_2 has reasonable accuracy for clinical use. Previous discussions on SvO_2 and its surrogate, $ScvO_2$, can be used for this purpose. Dueck et al.[9] investigated the bias and limits of agreement between $ScvO_2$ and SvO_2 in neurosurgical patients and found the largest 95% limits of agreement to be ±9.3%. They concluded that $ScvO_2$ values are not interchangeable with SvO_2, but they reported that the trend of the two parameters moved in the same direction. Reinhart et al.[11] also reported the limits of agreement between $ScvO_2$ and SvO_2 as 7.95% in critically ill patients. In our study, the 95% limits of agreement was 11.2% and was larger than the limits of agreement found in these previous studies. This finding suggests that the estimated SvO_2 values are not interchangeable with measured SvO_2. However, our results indicate that estimated SvO_2 demonstrates large changes when actual SvO_2 significantly changed. Rivers emphasized the importance of demonstrating trend of oxygen supply-demand relationship[19] and we believe that our methods also enable physicians to detect deteriorated oxygen supply-demand balance without a central venous catheter. Although this technique can only be applied to tracheally intubated and mechanically ventilated patients, we believe this possibility is especially useful for the anesthetic management of patients with limited cardiac reserve or significant intraoperative blood loss when central venous catheterization is not indicated.

In conclusion, we demonstrated that SvO_2 can be estimated from the data obtained by the NICO monitor, Hb concentration, and assumption of VCO_2/VO_2 ratio in mechanically ventilated patients. The data suggest that this estimation is not interchangeable with the SvO_2 value obtained from a PAC, but it can detect large changes of SvO_2. This method may provide an estimate of balance of oxygen supply and demand without inserting a central venous catheter.

APPENDIX: THE FORMULA TO ESTIMATE SVO_2 BY CO, VCO_2, AND HEMOGLOBIN CONCENTRATION

$$VO_2\,(mL/min) = DO_2\,(mL/min) - 1.36 \times Hb\,(g/dL) \times CO\,(L/min) \times SvO_2\,(\%) \times 0.1$$

$$VO_2\,(mL/min) = 1.36 \times Hb\,(g/dL) \times CO\,(L/min) \times SaO_2\,(\%) \times 0.1 - 1.36 \times Hb\,(g/dL) \times CO\,(L/min) \times SvO_2\,(\%) \times 0.1$$

If $SaO_2 = SpO_2$ and $VO_2\,(mL/min) = VCO_2\,(mL/min)/R$

R: respiratory quotient

$$VCO_2\,(mL/min)/R = 1.36 \times Hb\,(g/dL) \times CO\,(L/min) \times SpO_2\,(\%) \times 0.1 - 1.36 \times Hb\,(g/dL) \times CO\,(L/min) \times SvO_2\,(\%) \times 0.1$$

$$SvO_2 = SpO_2 - \frac{VCO_2\,(mL/min)/R}{1.36 \times Hb\,(g/dL) \times CO\,(L/min) \times 0.1}$$

If R can be estimated as 0.85,

$$SvO_2 = SpO_2 - \frac{VCO_2\,(mL/min)/0.85}{1.36 \times Hb\,(g/dL) \times CO\,(L/min) \times 0.1}$$

Adapted from Mark and Slaughter.[4]

REFERENCES

1. Vedrinne C, Bastien O, De Varax R, Blanc P, Durand PG, Du Gres B, Bouvier H, Saroul C, Lehot JJ. Predictive factors for usefulness of fiberoptic pulmonary artery catheter for continuous oxygen saturation in mixed venous blood monitoring in cardiac surgery. Anesth Analg 1997;85:2–10
2. Marx G, Reinhart K. Venous oximetry. Curr Opin Crit Care 2006;12:263–8
3. Rivers E, Nguyen B, Havstad S, Ressler J, Muzzin A, Knoblich B, Peterson E, Tomlanovich M. Early goal-directed therapy in the treatment of severe sepsis and septic shock. N Engl J Med 2001;345:1368–77
4. Mark JB, Slaughter TF. Cardiovascular monitoring. In: Miller RD, ed. Miller's anesthesia. 6th ed. Philadelphia: Elsevier Churchill Livingstone, 2005:1265–362
5. Levy RJ, Chiavacci RM, Nicolson SC, Rome JJ, Lin RJ, Helfaer MA, Nadkarni VM. An evaluation of a noninvasive cardiac output measurement using partial carbon dioxide rebreathing in children. Anesth Analg 2004;99:1642–7
6. Suzuki M, Koda S, Nakamura Y, Kawamura N, Shimada Y. The relationship between cardiac output measured by the thermodilution method and that measured by the carbon dioxide rebreathing technique during laparoscopic surgery. Anesth Analg 2005;100:1381–3
7. Bland JM, Altman DG. Measuring agreement in method comparison studies. Stat Methods Med Res 1999;8:135–60
8. Bland JM, Altman DG. Agreement between methods of measurement with multiple observations per individual. J Biopharm Stat 2007;17:571–82
9. Dueck MH, Klimek M, Appenrodt S, Weigand C, Boerner U. Trends but not individual values of central venous oxygen saturation agree with mixed venous oxygen saturation during varying hemodynamic conditions. Anesthesiology 2005;103:249–57
10. Pearse R, Dawson D, Fawcett J, Rhodes A, Grounds RM, Bennett ED. Changes in central venous saturation after major surgery, and association with outcome. Crit Care 2005;9:R694–R699
11. Reinhart K, Kuhn HJ, Hartog C, Bredle DL. Continuous central venous and pulmonary artery oxygen saturation monitoring in the critically ill. Intensive Care Med 2004;30:1572–8
12. Varpula M, Karlsson S, Ruokonen E, Pettila V. Mixed venous oxygen saturation cannot be estimated by central venous oxygen saturation in septic shock. Intensive Care Med 2006;32:1336–43
13. Sander M, Spies CD, Foer A, Weymann L, Braun J, Volk T, Grubitzsch H, von Heymann C. Agreement of central venous saturation and mixed venous saturation in cardiac surgery patients. Intensive Care Med 2007;33:1719–25
14. Levy RJ, Stern WB, Minger KI, Montenegro LM, Ravishankar C, Rome JJ, Nicolson SC, Jobes DR. Evaluation of tissue saturation as a noninvasive measure of mixed venous saturation in children. Pediatr Crit Care Med 2005;6:671–5
15. Wei W, Zhu Z, Liu L, Zuo Y, Gong M, Xue F, Liu J. A pilot study of continuous transtracheal mixed venous oxygen saturation monitoring. Anesth Analg 2005;101:440–3
16. Jones AE, Kuehne K, Steuerwald M, Kline JA. End expiratory oxygen concentrations to predict central venous oxygen saturation: an observational pilot study. BMC Emerg Med 2006;6:9
17. Tachibana K, Imanaka H, Miyano H, Takeuchi M, Kumon K, Nishimura M. Effect of ventilatory settings on accuracy of cardiac output measurement using partial CO_2 rebreathing. Anesthesiology 2002;96:96–102
18. Kotake Y, Moriyama K, Innami Y, Shimizu H, Ueda T, Morisaki H, Takeda J. Performance of noninvasive partial CO_2 rebreathing cardiac output and continuous thermodilution cardiac output in patients undergoing aortic reconstruction surgery. Anesthesiology 2003;99:283–8
19. Rivers E. Mixed vs central venous oxygen saturation may be not numerically equal, but both are still clinically useful. Chest 2006;129:507–8

Anesthesiology 2009; 111:818-25

Epidural Cooling Minimizes Spinal Cord Injury after Aortic Cross-clamping through Induction of Nitric Oxide Synthase

Akiko Ishikawa, M.D.,* Atsuo Mori, M.D.,† Nobuyuki Kabei, Ph.D.,‡ Akihiro Yoshitake, M.D.,§ Takeshi Suzuki, M.D.,* Nobuyuki Katori, M.D.,* Hiroshi Morisaki, M.D.,|| Ryohei Yozu, M.D.,# Junzo Takeda, M.D.**

Background: **By using a U-shaped lumen catheter, the authors examined the effects of epidural cooling on spinal cord injury after aortic cross-clamping (ACC), with a focus on changes of spinal cord blood flow and expression of inducible nitric oxide synthase.**

Methods: **Sixteen pigs were randomized into two groups: Control group (n = 8) or Cooling group (n = 8). In the latter, epidural cooling started at 30 min (baseline) before 45 min of ACC and persisted for the next 30 min of reperfusion period. Spinal cord blood flow and somatosensory-evoked potentials were assessed during peri-ACC period. At 48 h, we evaluated hind limb function by using Tarlov score and expression of inducible nitric oxide synthase on spinal cord using immunohistochemistry.**

Results: **After ACC, spinal cord blood flow dropped to a similar extent in both groups. During the reperfusion period, spinal cord blood flow increased up to 113% (103–124%), median (interquartile range), level transiently and decreased to 32% (22–47%) level *versus* baseline in the Control group, whereas it increased and remained at 92% (86–97%) level in the Cooling group. Simultaneously, somatosensory-evoked potentials showed that onset of loss time was delayed and recovery time was shortened in the Cooling group. Tarlov scores in the Cooling group were significantly higher and accompanied by normal-appearing motor neurons and significantly greater expression of inducible nitric oxide synthase on spinal cord *versus* the Control group.**

Conclusions: **This study shows that epidural cooling during ACC minimized the risk of spinal cord injury, possibly by preventing delayed hypoperfusion and upregulating inducible nitric oxide synthase expression.**

ALTHOUGH the outcome of surgical repair for throacoabdominal aortic aneurysm has been improved as a result of a marked advance of perioperative care and surgical techniques, paraplegia, occurring with high incidence between 6 and 16%, is not yet resolved as the most severe complication.[1,2] Although the underlying mechanisms remain to be fully determined, several factors, such as interruption of blood flow and/or increased cerebrospinal fluid pressure, have been proposed.[3] Clinically available protection of spinal cord consists of two approaches, *i.e.*, preservation of regional blood supply and reduction of oxygen demand during aortic cross-clamping (ACC). The former can be achieved with intercostal implantation, left heart bypass grafting, or cerebrospinal fluid drainage, whereas the latter with various pharmacologic agents and hypothermia.[3–5] Hypothermia is one of the most promising ways; however, given at systemic level detrimental complications such as coagulation abnormality, cardiac arrhythmia and pulmonary dysfunction could be unmasked.[6,7]

Cambria *et al.* demonstrated that regional hypothermia of spinal cord by infusion of iced saline into epidural space reduced spinal cord injury without systemic complications.[8] However, another concern has been raised to question whether this approach increases cerebrospinal fluid pressure associated with further deterioration of spinal cord perfusion. We, therefore, developed a newly designed epidural cooling catheter with closed perfusion circuit and demonstrated protective effects against spinal cord injury without elevating cerebrospinal fluid pressure.[9] Other investigators also described as a preliminary report that regional cooling with a closed perfusion system could be a good approach to prevent spinal cord injury during aortic surgery.[10] We, therefore, designed the current study to examine the effects of epidural cooling with focus on the changes of blood flow and somatosensory-evoked potentials (SEP) of spinal cord during peri-ACC periods, accompanied by evaluation of neurologic outcomes in a porcine model. In spinal cord injury induced by ischemia, activation of inducible nitric oxide synthase (iNOS) and subsequent nitric oxide production has been appreciated as a marker and therapeutic target.[11,12] Whereas two time periods of moderate to excessive nitric oxide discharge after spinal cord ischemia have been defined, *i.e.*, immediately after injury and several hours to days later, previous studies indicated that iNOS expression was mainly responsible for the latter.[13–15] In the current study, we therefore assessed histologic alterations concurrent with iNOS expression on spinal cord at 48 h after ischemic insults.

Materials and Methods

This experimental protocol was approved by the Animal Care Committee of Saitama Cardiovascular and Respiratory Center, Kumagaya, Saitama, Japan.

* Instructor, || Associate Professor, ** Professor, Department of Anesthesiology, § Instructor, # Professor, Department of Cardiovascular Surgery, Keio University School of Medicine; † Chief, Department of Cardiovascular Surgery, Kawasaki Municipal Hospital, Kanagawa; ‡ Chief Researcher, Saitama Cardiovascular and Respiratory Center, Saitama.

Received from Departments of Anesthesiology and Cardiovascular Surgery, Keio University School of Medicine, and Department of Cardiovascular Surgery, Kawasaki Municipal Hospital, and Saitama Cardiovascular and Respiratory Center, Japan. Submitted for publication March 9, 2009. Accepted for publication June 26, 2009. Support was provided solely from institutional and/or departmental sources. Presented in part at the Annual Meeting of American Society of Anesthesiologists, Orlando, Florida, October 21, 2008.

Address correspondence to Dr. Morisaki: Department of Anesthesiology, Keio University School of Medicine, 35 Shinanomachi, Shinjuku-ku, Tokyo 160-8582, Japan. morisaki@z8.keio.jp.

Animal Model and Preparatory Surgery

Male domestic pigs (40–50 kg) were studied after a 3- to 7-day period of acclimatization in our laboratory. The animals were initially anesthetized with intramuscular ketamine (10 mg/kg), and the trachea was intubated. With isoflurane anesthesia in oxygen, respiratory rate and tidal volume were adjusted to maintain normocapnia. Under the right lateral decubitus position, a cooling-warming blanket was applied to maintain rectal temperature at approximately 36°C throughout the study periods. An epidural cooling catheter (Unitika, Tokyo, Japan), which was developed by our group,[9] was inserted at L2 level *via* laminectomy and removal of ligamentum fluvum. The catheter has 16-gauge outer diameter and 35-cm length and a closed countercurrent lumen, allowing fluid to circulate the inside. The tip of catheter directed into cephalad of epidural space was placed at Th6 level, which was confirmed for each animal by using an x-ray examination. The other side of this catheter was connected to an external roller pump and heat exchanger (MERA modular type and CP-4; Senko Medical Instrument, Tokyo, Japan), which enabled cooled-saline to circulate inside the catheter (fig. 1). Epidural cooling catheter, cooling unit, and circulating pump made up the circuit. Distilled water was not infused into epidural space directly but was circulated as a coolant within the U-shaped lumen of epidural catheter and extracorporeal circuit. This system and an epidural catheter with closed countercurrent lumen could provide regional cord cooling without increasing intrathecal pressure as described previously.[9] Bipolar electrodes for monitoring of SEP were placed in epidural space at L4/5 level for stimulation and at Th5/6 level for record. To continuously monitor epidural and subarachnoidal temperatures, thermistor probes were placed on dorsal dura and in subarachnoid space at L3 level. Arterial catheters were inserted in right axillary artery (proximal to clamp site) and right femoral artery to measure arterial blood pressure (distal to clamp site), respectively. Heart rate and rectal temperature were continuously monitored throughout the study periods.

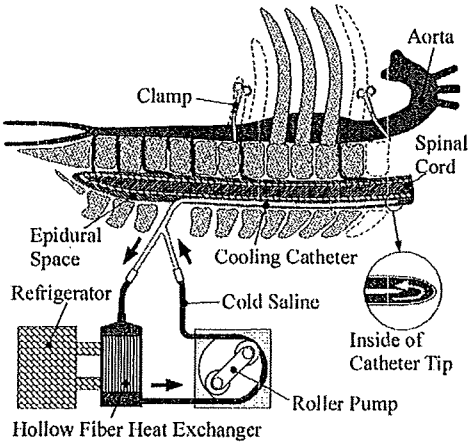

Fig. 1. Schematic drawing of continuous cord cooling system and epidural cooling catheter with a closed countercurrent lumen.

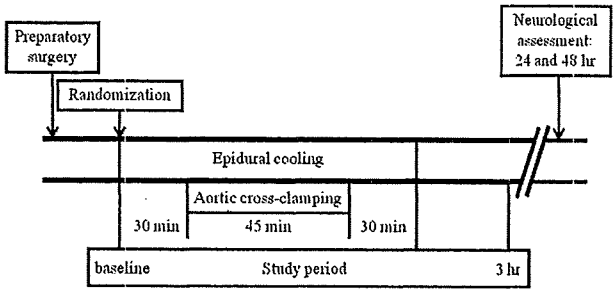

Fig. 2. Study protocol.

Study Protocol

After the placement of epidural cooling and monitoring catheters, 16 domestic pigs were randomly allocated into two groups by using a computer-generated random number. Control group (n = 8) received placement of an epidural catheter alone, Cooling group (n = 8) received regional cooling by continuous cord cooling system with an epidural cooling catheter (fig. 2). The animals then underwent thoracotomy at the fourth and seventh intercostals under sterile conditions. After surgical preparation for ACC, heparin sulfate (60 U/kg) was injected to provide systemic anticoagulation. In Cooling group, epidural cooling by circulating cooled saline (4°C) at a rate of 75–90 ml/min was started 30 min before ACC and continued until 30 min after ACC (105 min for total epidural cooling time). All animals underwent segmental ACC for 45 min between the distal site to left subclavian artery and the proximal site to the diaphragm. Complete ACC was confirmed by the loss of femoral artery pressure (distal blood pressure) during ACC. Transient hypertension detected at the right axillary artery after ACC was regulated with intermittent injection of intravenous nicardipine hydrochloride. Blood pressure after declamping was maintained with fluid resuscitation and intravenous injection of phenylephrine hydrochloride. After a 3-h examination period, all catheters and monitors were removed and wounds were closed. When emergence from anesthesia was achieved, the trachea was extubated, and the animal was returned to the cage for subsequent examination of neurologic outcome in hind limb for 48 h.

Measurements of Blood Flow and SEP of Spinal Cord

Blood flow to spinal cord (SCBF) was continuously measured by using laser-Doppler flowmetry (Model LBF-III; Biomedical Science, Tokyo, Japan) adjusted for high-flow measurement (12 kHz, gain 1 or 3) and a time constant of 3.0 s. The signal was continuously recorded on a 2-channel strip-card recorder and referred to as SCBF. The tip of laser-Doppler probe was implanted on the epidural surface at L2 level, because porcine spinal

cord extends at L6[16] and preservation of spinal cord under physiologic state is consequential. In our pilot study, we measured both direct and transepidural spinal cord blood flow simultaneously by using two independent laser-Doppler probes placed on dorsal lumbar spinal cord and epidural space at 2 mm apart, and we found that the change of direct measurement was correlated well with indirect approach, *i.e.*, transepidural measurements of spinal cord blood flow. Characteristics of translucent dura with few vessels in pigs[17,18] accompanied by capability of laser-Doppler to measure up to 1 mm in depth[19] allowed us to measure accurate and real-time alterations of SCBF.

We simultaneously examined SEP directly derived from spinal cord. Stimulation was given with 0.2-ms pulse duration and 3- to 5-mÅ current with a rate of 5.0 Hz (Neuropack; Nihon Kohden, Tokyo, Japan). Potentials were recorded on a time base of 3 ms after passing through a bandpass filter of 50 to 1500 Hz. Each record represented an average of 50 repetitions. A baseline SEP was recorded before the initiation of epidural cooling, and the recording was repeated at 60-s intervals. Signal amplitude and latency of each SEP were recorded and compared to the baseline.

Neurologic and Histologic Assessments

Hind limb motor function was evaluated at 24 and 48 h after the ACC by using a modified Tarlov score (0 = complete paralysis, 1 = minimal movement, 2 = standing with assistance, 3 = standings alone but unable to walk, 4 = weak walking, 5 = full recovery with normal walking).[20,21]

After neurologic examination at 48 h, the animals were sacrificed with an overdose injection of sodium pentobarbital. Spinal cord was removed immediately and fixed in 10% formaldehyde solution. Spinal cord at L4 level was sliced into sections, and each section was stained with hematoxylin and eosin. Ten slices per animal were examined for histologic assessment. A pathologist who was unaware of the study protocol and neurologic outcome of the animals examined each slice by light microscopy and counted the total number of motor neurons (larger than 50 μm in diameter) with normal appearance. Simultaneously, histologic alterations to reflect inflammatory responses of ischemic spinal cord injury such as proliferation of microglia cells at perivascular area and formation of hydropic vacuolation were assessed as described previously.[22,23]

Immunohistochemical Staining of Spinal Cord

Spinal cord fixed with 10% formalin and embedded with paraffin were sectioned into 4 μm^2. After de-waxing with xylene and rehydrating with methanol, these sections were heat-treated in 10 mM citrate buffer (pH 6.0) at 105°C for 10 min and then washed with Tris-buffered saline three times for 5 min. Specimen was blocked with Image-iT FX (Tokyo, Japan) for 30 min. After washing, iNOS (Epitope-specific rabbit antibody, LVC; Lab Vision Corp., Fremont, CA) and normal rabbit immunoglobulin (control antibody, Vector) were incubated for 60 min at room temperature. After washing with Tris-buffered saline-Tween 20, each section was treated with Alexa Fluor 488-conjugated goat anti-rabbit antibody (Invitrogen; Carlsbad, CA). After washing with Tris-buffered saline-Tween 20, the sections were counterstained and mounted with an antifade reagent (ProLong Gold®, Invitrogen) and 4′,6-diamidino-2-phenylindole.

The level of iNOS expression on spinal cord was determined by digital imaging after immunofluorescence. Images were taken by using epifluorescent microscopy with Applied Imaging Ariol® SL-50 system (Genetix, Hampshire, United Kingdom) equipped with magnification of 40× objective. The slide which has maximum signal to noise ratio in caudal extremity in spinal cord were manually selected. In selected slides, the optimal exposure time of acquisition was set with a highly sensitive charge-coupled device camera. Then, the images of iNOS expressed were obtained from all specimens with the same acquisition setting and were depicted by pseudo color merging with image processing software ImageJ (National Institutes of Health, Bethesda, MD). Color-merged Red-Green-Blue images were split into each 8-bit gray channel with ImageJ. Motor neuron in each image was selected as measurement region of interest. Signals of iNOS were extracted from background noise subtraction with threshold adjustment in binary images. Target average intensities were measured with ImageJ measurement and were indicated as histogram.

Statistical Analysis

Data were presented as median and interquartile range unless otherwise specified, and Mann–Whitney U-test was applied by using a statistical software package of SPSS/15.0J for Windows (SPSS Inc., Chicago, IL). In all cases, two-tailed P value less than 0.05 was considered significant.

Results

All animals in both study groups survived for 48-h study periods, and no animal was excluded from the analyses.

Changes of Epidural and Subarachnoidal Temperatures and SCBF during Peri-ACC Periods

Rectal temperatures in both the Control and Cooling groups remained around 36°C (36.1 ± 0.4°C and 36.2 ± 0.4°C, respectively; mean ± SD) throughout the study periods. In the Control group, both epidural and subarachnoidal temperatures were kept within comparable ranges with the ranges of rectal temperatures (fig. 3A).

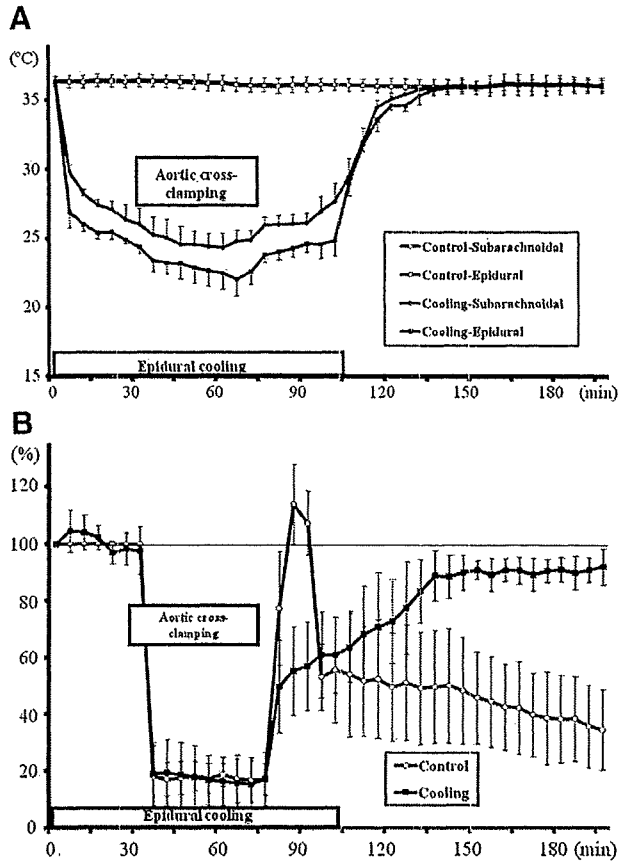

Fig. 3. (*A*) Changes in subarachnoidal and epidural temperatures during peri-aortic cross-clamping periods in the Control and Cooling groups. Note that both epidural and subarachnoidal temperatures in the Cooling group were kept less than 26°C during aortic cross-clamping. Values are mean (SD). (*B*) Changes in spinal cord blood flow (SCBF) during peri-aortic cross-clamping periods in Control and Cooling groups. Values are mean (SD). Note that SCBF in both groups were kept at approximately 20% level during aortic cross-clamping *versus* baseline, and that SCBF in the Control group increased up to 114% and gradually decreased to 34% level after de-clamping, whereas it increased in the Cooling group and remained at 92% level throughout the study period.

On the other hand, epidural temperature in the Cooling group dropped immediately after initiating epidural cooling and kept approximately 24–26°C ranges during ACC. Simultaneously, subarachnoidal temperature in the Cooling group reached 26°C level and stayed between 26 and 28°C. After the end of epidural cooling, both temperatures in the Cooling group increased gradually up to the baseline level.

Figure 3B illustrates the changes of SCBF during peri-ACC periods. The SCBF that were comparable between the groups during the 30-min perfusion period until ACC dropped to a similar extent (18–20% level *vs.* baseline) immediately after ACC. During reperfusion period, the SCBF in the Control group was increased up to 114% (103–124%) level within 10 min and then rapidly dropped to approximately 50% level, subsequently decreased to 32% (22–47%) level for the next 100 min

Table 1. Loss and Recovery of Spinal Cord Somatosensory-evoked Potentials in the Control and Cooling Groups

	Control Group	Cooling Group	*P* Value
Onset of SEP loss, min	12.9 (9.6–13.7)	26.5 (22.3–30.0)	0.0008
Total duration of SEP loss, min	41.9 (37.2–43.8)	21.3 (20.4–25.9)	0.0008
Recovery time of SEP, min	6.9 (5.7–9.9)	3.2 (2.4–4.2)	0.0023

Data were expressed as median (interquartile range). Mann-Whitney U-test was used to compare the difference between the groups.
SEP = spinal cord somatosensory-evoked potentials.

versus the baseline. On the contrary, SCBF after de-clamping in the Cooling group increased gradually and remained over 92% (86–97%) level throughout the reperfusion period.

SEP of Spinal Cord and Neurologic Outcome

No animal showed the abortion of SEP waveform as a result of epidural cooling itself. During epidural cooling before ACC, latency of SEP was prolonged, but its amplitude remained unchanged. Onset time of SEP loss after ACC was significantly longer in the Cooling *versus* the Control group, whereas total duration of SEP loss in the Cooling group was significantly shorter *versus* the Control group (table 1). In addition, recovery time of SEP after de-clamping was significantly shorter in the Cooling group *versus* Control group.

Figure 4 illustrates the data of neurologic outcome by scoring hindlimb function at 24 and 48 h after ACC. The animals in the Cooling group showed significantly better Tarlov scores at 24 and 48 h *versus* the Control group (Mann–Whitney U-test $P = 0.0003$ and 0.0004, respectively). Besides, the total number of intact motor neu-

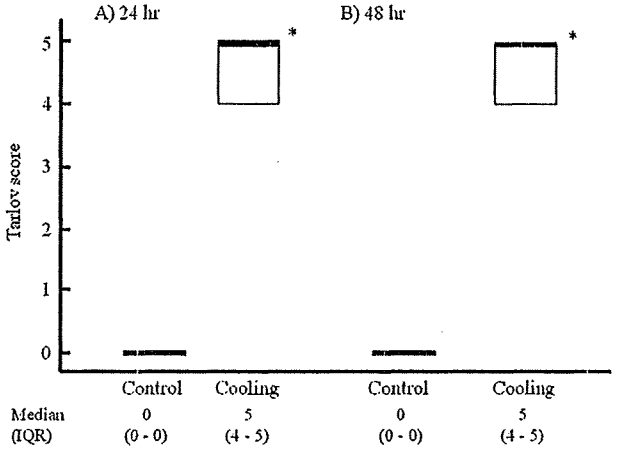

Fig. 4. Neurologic outcome scores of hind limb at 24 and 48 h after aortic cross-clamping. *Boxes* represent the interquartile range (IQR) containing 50% of the values. *Horizontal thick lines* indicate the median values. * Significantly different from the Control group; Tarlov scores in the Cooling group were significantly better than those in the Control group at both 24 and 48 h (Mann–Whitney U-test $P = 0.0003$ and $P = 0.0004$, respectively).

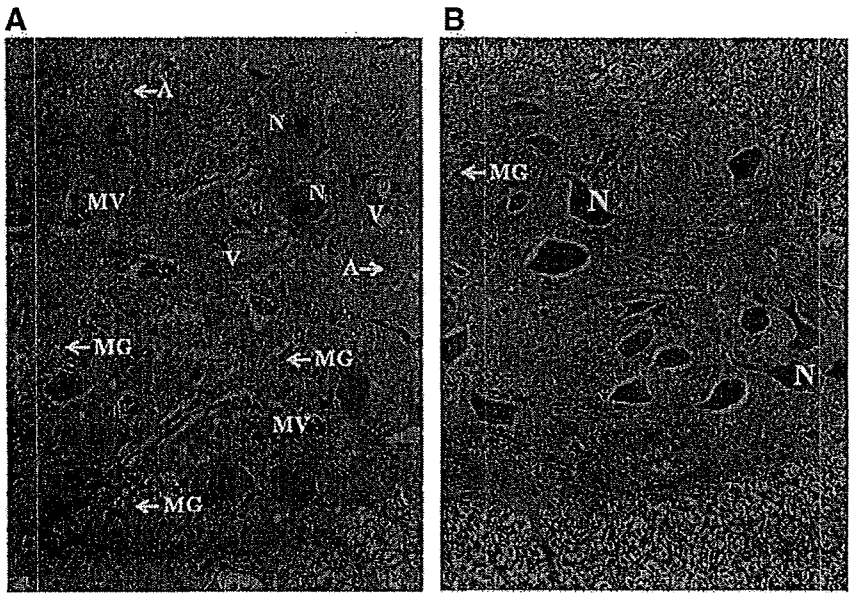

Fig. 5. Representative microphotographs of anterior horn of spinal cord stained with hematoxyline and eosin (original magnification ×10). (*A*) A representative picture in the Control group. Note that severe necrosis was found as swollen motor neurons with no Nissl granules (N) and that inflammatory alterations and edema formation were observed as proliferation of microglias (MG), swollen astrocytes (A), and microvessels (MV) and profound hydropic vacuolation (V). Almost half of motor neurons were pathologically lost in the Control group. (*B*) A representative picture in the Cooling group. Note that nearly normal appearance of motor neurons with Nissl granules (N) and few microglias (MG) were found.

rons per each section was significantly greater in the Cooling *versus* the Control group (123 [117–126] *vs.* 66 [52–75]: Mann–Whitney U-test $P = 0.0001$), indicating that almost half of motor neurons were lost in the Control group.

Histopathological Alterations and Expression of iNOS in Spinal Cord

Figures 5A and 5B show representative microphotographs of anterior horn of spinal cord in both the Control and Cooling groups. Nearly normal appearance of motor neurons with Nissl granules and glia cells were found in the Cooling group (panel B), whereas severe necrosis of motor neurons accompanied by a moderate level of hydropic vacuolation and apparent gliosis, *i.e.*, proliferation of astrocytes and microglia cells, and vascularization was observed in the Control group (panel A).

Figures 6A and 6B illustrate the representative microscopic images of positive immunostaining iNOS expression on spinal cord in both study groups. The extent of iNOS expression and the number of motor neurons were apparently augmented in the Cooling group *versus* the Control group. Figure 6C demonstrates histogram of iNOS expression of spinal cord in both study groups quantitatively assessed using ImageJ. The expression of iNOS was significantly augmented in the Cooling group *versus* the Control group (Mann–Whitney U-test $P = 0.012$).

Discussion

By using a porcine model of ACC, we demonstrated that epidural cooling catheter with closed circuit lumen preserved regional hypothermia of spinal cord approximately at 26°C and completely prevented the development of paraplegia at 48 h. We also showed that epidural cooling prevented reactive hyperemia and delayed hypoperfusion of SCBF after ACC, accompanied by apparent reduction of histologic alterations such as necrosis of motor neurons, hydropic vacuolation, and proliferation of microglia cells and microvessels. Simultaneously, regional epidural cooling during ACC augmented the induction of iNOS in motor neurons at 48 h after ischemic insult, which could be associated with the improvement of neurologic outcomes. Although its protective property against delayed-onset paraplegia remains to be determined,[24] the current study shed light on clinical application of this continuous cord cooling system in patients undergoing thoracoabdominal surgery.

Because of its similarities of anatomical characteristics and hemodynamic responses to human as well as its reproducibility of paraplegia, the porcine model has been widely used for examination of spinal cord injury and validation of protective strategy during ACC.[25] In the current study, ACC induced abrupt reduction of SCBF irrespectively from epidural cooling, whereas approximately 20% level of baseline SCBF was preserved during ACC (fig. 3B), indicating that SCBF was in part supplied by collateral vessels[26] and that paraplegia observed in the Control group was not fully attributed to complete block of blood flow during ACC. Although our approach for blood flow measurement does not directly reflect the ventral side of spinal cord, where vulnerable motor neurons are rich, previous study demonstrated that there were no differences in blood flow among different areas of spinal cord during insults.[27,28] In addition, some may argue that motor-evoked potentials rather than SEP, mediated through posterior and lateral column of spinal cord, could be more reasonable for the assessment of ischemic spinal cord.[29] Due to its lesser sensitivity to

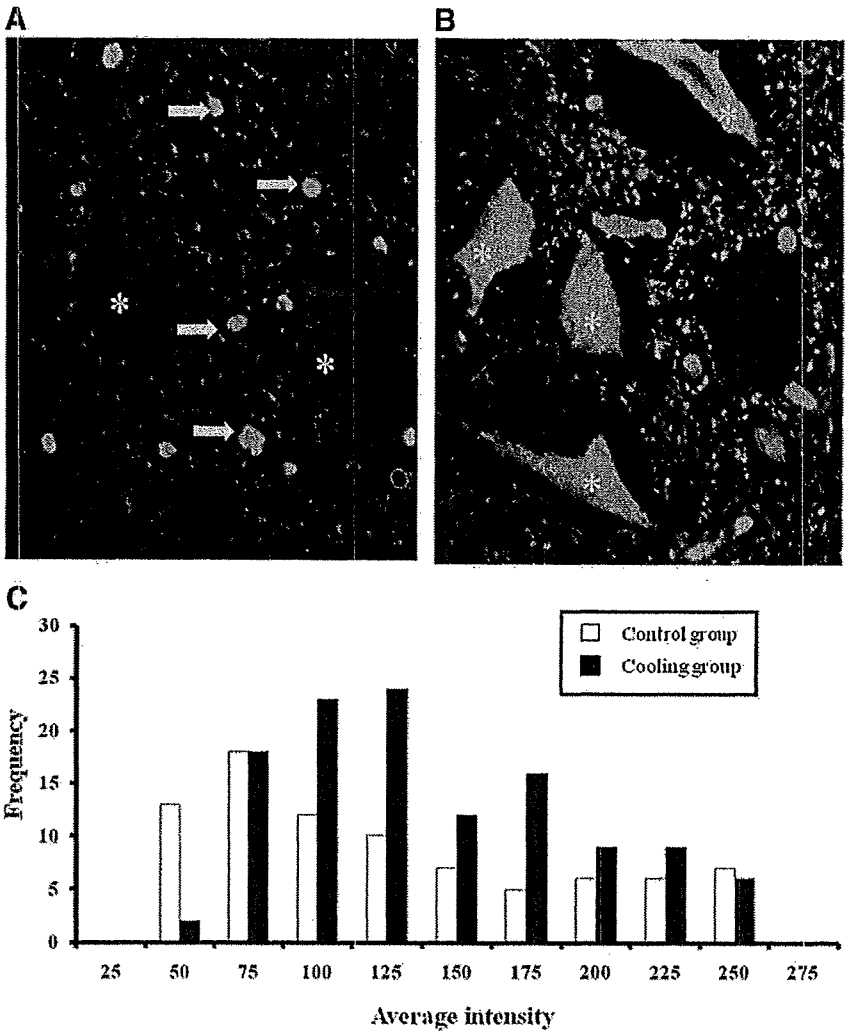

Fig. 6. Immunohistochemical staining of spinal cord for inducible nitric oxide synthase (iNOS) (magnification ×40) and histogram of average intensity of iNOS expression in ventral gray matter. (*A*) A representative picture of the Control group. Positive staining for iNOS is *green*. Note that iNOS expression was found in proliferated glia cells (*arrow*) and that motor neurons were obviously swollen without iNOS expression (*asterisk*). (*B*) A representative picture of the Cooling group. Positive staining for iNOS is *green*. Note that iNOS was expressed in motor neurons (*asterisk*), which have normal architecture, and that no proliferation of glia cells was found. (*C*) Histogram of average intensity of iNOS expression in ventral gray matter of spinal cord. Average intensity in the Cooling group was significantly augmented *versus* the Control group ($P = 0.01275$).

volatile anesthetics, more feasibility in clinical settings, and compatibility with motor-evoked potentials to predict paralysis during ACC,[30,31] however, we used SEP during spinal cord ischemia in this study. We then found that total time of SEP loss could predict a risk of paraplegia more reliably than the amplitude of recovery wave. On the other hand, the time to loss of SEP observed in the Cooling group was twice as much *versus* the Control group, indicating that functional activity of neuronal cells assessed by SEP was not always dependent on the amount of blood supply. Previous study also showed that the time to loss of SEP and the time required for SEP recovery reflected neurologic outcomes of motor function.[32,33]

As a postischemic common phenomenon, reactive hyperemia, defined as transient augmentation of blood supply to tissues after ischemic insults, could be the major trigger to evoke tissue edema and organ dysfunction through excessive discharges of oxidative species and other mediators.[23] Indeed, paraplegia is directly correlated with the extent of reactive hyperemia,[34] which response found in our study appeared to be too small compared to previous reports. Barone *et al.* demonstrated that eight times greater extent of hyperemia *versus* baseline induced apparent edema of spinal cord and paraplegia and that 200% level of augmented blood flow was not high enough to evoke apparent paraplegia after spinal cord ischemia.[35] On the contrary, other studies demonstrated that delayed hypoperfusion *per se* was more consequential to modulate the size of cerebral infarction[36,37] and to develop structural alterations of spinal cord, including hydropic vacuolation and proliferation of microglia cells and microvessels, accompanied by swollen motor neurons as observed in the Control group (fig. 5A).[22,38] Collectively, prevention of delayed hypoperfusion could be a prevailing component of epidural cooling properties to protect spinal cord from ischemic injury.

Another important finding of this study is that epidural cooling augmented the expression of iNOS on spinal cord *versus* the Control group. Spinal cord injury after ACC is basically caused by both primary injury associated with severe reduction of SCBF and secondary injury associated with free radical production, intracellular cal-

cium mobilization, and/or excessive nitric oxide production.[12,22] To protect spinal cord from ischemic injury, therefore, it is crucial to reestablish normal SCBF as quickly as possible and to simultaneously prevent the progression of secondary cascades. However, since a marked expression of iNOS was unveiled more than 24 h after ischemic insults in central nervous system,[11,39,40] prevention of reactive hyperemic response and delayed hypoperfusion during the early phase after ischemic insults observed in the Cooling group cannot be accounted for by iNOS activation, but possibly by other types of nitric oxide synthase, such as neuronal or endothelial.[14] On the other hand, a marked iNOS expression with subsequent nitric oxide discharges *in situ* could be associated with the prevention of secondary injury in the Cooling group. Previous study demonstrated that protective effects of volatile anesthetics on spinal cord ischemia were mediated by nuclear factor-κB-dependent pathway, *i.e.*, secondary pro-inflammatory pathway.[41] Another report using a mesenteric ischemia-reperfusion model indicated that topical hypothermia prevented both nuclear factor-κB activation and iNOS expression, accompanied by significant reduction of increased intestinal permeability and histologic injury.[42] On the basis of the clear difference of neurologic outcomes, augmented iNOS expression in the Cooling group (fig. 6A) is likely to provide its protective properties on ischemic spinal cord, possibly through the inhibition of secondary cascade rather than the immediate restoration of blood flow.

Although there is ongoing controversy regarding the roles of nitric oxide in ischemia-reperfusion injury,[14] double-sward action of nitric oxide depends on the cell type from which nitric oxide is released, the type of nitric oxide synthase, the time period after ischemia, or the severity of ischemic insult.[43] Previous study showed that cerebral infarct size and degree of motor deficit produced by artery occlusion were smaller in iNOS knockout mouse.[39] In addition, expression of iNOS in microglial cells observed in the Control group was shown to initiate neurotoxic process and subsequent neuronal death, possibly through increased susceptibility to glutamate.[44,45] Others showed that induction of iNOS in motor neurons in ventral horn appeared to be protective despite depending on the amount of nitric oxide discharges.[11] Although it remains to be fully clarified, either iNOS expression in intact motor neurons or inhibition of glia-derived nitric oxide production could serve to protect spinal cord from ischemic insults, subsequently improving neurologic outcomes in the Cooling group. Previous study demonstrated that expression of iNOS after ischemic injury in central nervous system stimulated neurogenesis,[46] indicating that iNOS expression might not be the results of acute inflammatory response against ischemia-reperfusion but consequential process to restore injured neurons. Nevertheless, further investigation should be warranted to clarify the roles of different types of nitric oxide synthase at the early and late phases of spinal cord injury by using a specific inhibitor.[39]

In conclusion, regional epidural cooling during peri-ACC period minimized both functional and structural alterations of spinal cord and thereby improved neurologic outcome possibly through prevention of delayed hypoperfusion and augmentation of iNOS expression.

The authors gratefully thank Naoki Tomotsugu, B.A., Research Associate, Clinical Research Center, Keio University School of Medicine, Tokyo, Japan, for his great help with statistical analyses, Takashi Kimura, Technician, Tokyo Electric Power Hospital, Tokyo Japan, for his help with pathological analyses, and Ryoichi Tashiro, Ph.D., Researcher, Saitama Cardiovascular and Respiratory Center, Saitama, Japan, Setsuko Misawa, Technician, Saitama Cardiovascular and Respiratory Center, Saitama, Japan, and Takeshi Yokomura, Technician, Saitama Cardiovascular and Respiratory Center, Saitama, Japan for their excellent technical assistance.

References

1. Crawford ES, Crawford JL, Safi HJ, Coselli JS, Hess KR, Norton HJ, Glaeser DH: Thoracoabdominal aortic aneurysms: Preoperative and intraoperative factors determining immediate and long-term results of operations in 605 patients. J Vasc Surg 1986; 3:389-404
2. Svensson LG, Crawford ES, Hess KR, Coselli JS, Safi HJ: Experience with 1509 patients undergoing thoracoabdominal aortic operations. J Vasc Surg 1993; 17:357-70
3. Ling E, Arellano R: Systematic overview of the evidence supporting the use of cerebrospinal fluid drainage in thoracoabdominal aneurysm surgery for prevention of paraplegia. Anesthesiology 2000; 93:1115-22
4. Acher CW, Wynn MM, Hoch JR, Popic P, Archibald J, Turnipseed WD: Combined use of cerebral spinal fluid drainage and naloxone reduces the risk of paraplegia in thoracoabdominal aneurysm repair. J Vasc Surg 1994; 19:236-4
5. Kouchoukos NT, Daily BB, Rokkas CK, Murphy SF, Bauer S, Abboud N: Hypothermic bypass and circulatory arrest for operations on the descending thoracic and thoracoabdominal aorta. Ann Thorac Surg 1995; 60:67-77
6. Rohrer MJ, Natale AM: Effect of hypothermia on the coagulation cascade. Crit Care Med 1992; 20:1402-5
7. Kurz A, Sessler DI, Lenhardt R, The Study of Wound Infection and Temperature Group: Perioperative normothermia to reduce the incidence of surgical-wound infection and shorten hospitalization. N Engl J Med 1996; 334:1209-15
8. Cambria RP, Davidson JK, Zannetti S, L'Italien G, Brewster DC, Gertler JP, Moncure AC, LaMuraglia GM, Abbott WM: Clinical experience with epidural cooing for spinal cord protection during thoracic and thoracoabdominal aneurysm repair. J Vasc Surg 1997; 25:234-43
9. Yoshitake A, Mori A, Shimizu H, Ueda T, Kabei N, Hachiya T, Okano H, Yozu R: Use of an epidural cooling catheter with a closed countercurrent lumen to protect against ischemic spinal cord injury in pigs. J Thorac Cardiovasc Surg 2007; 134:1220-6
10. Moomiale RMA, Ransden J, Stein J, Strugar J, Zhu QB, Kim JH, Elefteriades JA: Cooling catheter for spinal cord preservation in thoracic aortic surgery. J Cardiovasc Surg 2007; 48:103-8
11. Zhou Y, Zhao YN, Yang EB, Ling EA, Wang Y, Hassouna MM, Mack P: Induction of neuronal and inducible nitric oxide synthase in the motoneurons of spinal cord following transient abdominal aorta occlusion in rats. J Surg Res 1999; 87:185-93
12. Beattie MS: Inflammation and apoptosis: linked therapeutic targets in spinal cord injury. Trends Mol Med 2004; 10:580-3
13. Nakahara S, Yone K, Setoguchi T, Yamaura I, Arishima Y, Yoshino S, Komiya S: Changes in nitric oxide and expression of nitric oxide synthase in spinal cord after acute traumatic injury in rats. J Neurotrauma 2002; 19:1467-74
14. Conti A, Miscusi M, Cardali S, Germanò A, Suzuki H, Cuzzocrea S, Tomasello F: Nitric oxide in the injured spinal cord: Synthases cross-talk, oxidative stress and inflammation. Brain Res Rev 2007; 54:205-18
15. Pannu R, Singh I: Pharmacological strategies for the regulation of inducible nitric oxide synthase: Neurodegenerative *versus* neuroprotecive mechanisms. Neurochem Intern 2006; 49:170-82
16. Mok JM, Lyon R, Lieberman JA, Cloyd JM, Burch S: Monitoring of nerve root injury using transcranial motor-evoked potentials in a pig model. Spine 2008; 33:E465-73
17. Lips J, de Haan P, Bouma GJ, Jacobs MJ, Kalkman CJ: Delayed detection of motor pathway dysfunction after selective reduction of thoracic spinal cord blood flow in pigs. J Thorac Cardiovasc Surg 2002; 123:531-8
18. Orlin JR, Osen KK, Hovig T: Subdural compartment in pig: A morphologic study with blood and horseradish peroxidase infused subdurally. Anat Rec 2005; 230:22-37

19. Nilsson GE, Tenland T, Obert PA: A new instrument for continuous measurement of tissue blood flow by light beating spectroscopy. IEEE Trans Biomed Eng 1980; 27:12-9

20. Tarlov IM: Acute spinal cord compression paralysis. J Neurosurg 1972; 36:10-20

21. Mori A, Ueda T, Hachiya T, Kabei N, Okano H, Yozu R, Sasaki T: An epidural cooling catheter protects the spinal cord against ischemic injury in pigs. Ann Thorac Surg 2005; 80:1829-34

22. Dumont RJ, Okonkwo DO, Verma S, Hurlbert RJ, Boulos PT, Ellegala DB, Dumont AS: Acute spinal cord injury, part I: Pathophysiologic mechanisms. Clin Neuropharmacol 2001; 24:254-64

23. Jacobs TP, Shohami E, Baze W, Burgard E, Gunderson C, Hallenbeck JM, Feuerstein G: Deteriorating stroke model: Histopathology, edema, and eicosanoid changes following spinal cord ischemia in rabbits. Stroke 1987; 18:741-50

24. Wong DR, Coselli JS, Amerman K, Bozinovski J, Carter SA, Vaughn WK, LeMaire SA: Delayed spinal cord deficits after thoracoabdominal aortic aneurysm repair. Ann Thorac Surg 2007; 83:1345-55

25. Strauch JT, Spielvogel D, Lauten A, Zhang N, Shiang H, Weisz D, Bodian CA, Griepp RB: Importance of extrasegmental vessels for spinal cord blood supply in a chronic porcine model. Eur J Cardio-thorac Surg 2003; 24:817-24

26. Taira Y, Marsala M: Effect of proximal arterial perfusion pressure on function, spinal cord blood flow, and histopathologic changes after increasing intervals of aortic occlusion in the rat. Stroke 1996; 27:1850-8

27. Hayashi T, Sakurai M, Abe K, Sadahiro M, Tabayashi K, Itoyama Y: Apoptosis of motor neurons with induction of caspases in the spinal cord after ischemia. Stroke 1998; 29:1007-13

28. Jacobs TP, Kempski O, McKinley D, Dutka AJ, Hallenbeck JM, Feuerstein G: Blood flow and vascular permeability during motor dysfunction in a rabbit model of spinal cord ischemia. Stroke 1992; 23:367-73

29. Strauch JT, Lauten A, Spielvogel D, Rinke S, Zhang N, Weisz D, Bodian CA, Griepp RB: Mild hypothermia protects the spinal cord from ischemic injury in a chronic porcine model. Eur J Cardio-thorac Surg 2004; 25:708-15

30. Shine TSJ, Harrison BA, De Ruyter ML, Crook JE, Heckman M, Daube JR, Stapelfeldt WH, Cherry KJ, Gloviczki P, Bower TC, Murray MJ: Motor and somatosensory evoked potentials. Their role in predicting spinal cord ischemia in patients undergoing thoracoabdominal aortic aneurysm repair with regional lumbar epidural cooling. Anesthesiology 2008; 108:580-7

31. Kahn RA, Stone ME, Moskowitz DM: Anesthetic consideration for descending thoracic aortic aneurysm repair. Sem Cardiothorac Vasc Anesth 2007; 11: 205-23

32. Grabitz K, Sandmann W, Stühmeier K, Mainzer B, Godehardt E, Ohre B, Hartwich U: The risk of ischemic spinal cord injury in patients undergoing graft replacement for thoracoabdominal aortic aneurysms. J Vasc Surg 1996; 23: 230-40

33. Laschinger JC, Cunningham JN, Cooper MM, Baumann FG, Spencer FC: Monitoring of somatosensory evoked potentials during surgical procedures on the thoracoabdominal aorta. I. Relationship of aortic cross-clamp duration, changes in somatosensory evoked potentials, and incidence of neurologic dysfunction. J Thorac Cardiovasc Surg 1987; 94:260-5

34. Svensson LG, Hunter SJS, Von Ritter CM, Robinson MF, Groeneveld HT, Hinder RA, Rickards ES: Cross clamping of the thoracic aorta: Influence of aortic shunts, laminectomy, papaverine, calcium channel blocker, allopurinol, and superoxide dismutase on spinal cord blood flow and paraplegia in baboons. Ann Surg 1986; 204:38-47

35. Barone GW, Joop AW, Flanagan TL, Dunn CE, Kron IL: The effect of hyperemia on spinal cord function after temporary thoracic aortic occlusion. J Vasc Surg 1988; 8:535-40

36. Steen PA, Newberg LA, Milde JH, Michenfelder JD: Nimodipine improves cerebral blood flow and neurologic recovery after complete cerebral ischemia in the dog. J Cereb Blood Flow Metab 1983; 3:38-43

37. Meyer FB, Anderson RE, Friedrich PF: MK-801 attenuates capillary bed compression and hypoperfusion following incomplete focal cerebral ischemia. J Cereb Blood Flow Metab 1990; 10:895-902

38. Papakostas JC, Matsagas MI, Toumpoulis IK, Malamou-Mitsi VD, Pappa LS, Gkrepi C, Anagnostopoulos CE, Kappas AM: Evolution of spinal cord injury in a porcine model of prolonged aortic occlusion. J Surg Res 2006; 133:159-66

39. Iadecola C, Zhang F, Xu X: Inhibition of inducible nitric oxide synthase ameliorates cerebral ischemic damage. Am J Phsyiol 1995; 268:R286-92

40. Hamada Y, Ikata T, Katoh S, Tsuchiya K, Niwa M, Tsutsumishita Y, Fukuzawa K: Roles of nitric oxide in compression injury of rat spinal cord. Free Radic Biol Med 1996; 20:1-9

41. Kim H, Yi JW, Sung YH, Kim CJ, Kim CS, Kang JM: Delayed preconditioning effect of isoflurane on spinal cord ischemia in rats. Neurosci Lett 2008; 440:211-6

42. Hassoun HT, Kozar RA, Kone BC, Safi HJ, Moore FA: Intraischemic hypothermia differentially modulates oxidative stress proteins during mesenteric ischemia/reperfusion. Surgery 2002; 132:369-76

43. Iadecola C: Bright and dark sides of nitric oxide in ischemic brain injury. Trends Neurosci 1997; 20:132-9

44. Bolaños JP, Almeida A: Roles of nitric oxide in brain hypoxia-ischemia. Biochim Biophys Acta 1999; 1411:415-36

45. Zhao W, Xie W, Le W, Beers DR, He Y, Henkel JS, Simpson EP, Yen AA, Xiao Q, Appel SH: Activated microglia initiate motor neuron injury by a nitric oxide and glutamate-mediated mechanism. J Neuropathol Exp Neurol 2004; 63:964-77

46. Zhu DY, Liu SH, Sun HS, Lu YM: Expression of inducible nitric oxide synthase after focal cerebral ischemia stimulates neurogenesis in the adult rodent dentate gyrus. J Neurosci 2003; 23:223-9

UICC
global cancer control

International Journal of Cancer

ADAM28 is a serological and histochemical marker for non-small-cell lung cancers

Hiroaki Kuroda[1,2], Satsuki Mochizuki[1], Masayuki Shimoda[1], Miyuki Chijiiwa[1], Kazunori Kamiya[1,2], Yotaro Izumi[2], Masazumi Watanabe[2], Hirohisa Horinouchi[2], Masahumi Kawamura[2], Koichi Kobayashi[2] and Yasunori Okada[1]

[1] Department of Pathology, School of Medicine, Keio University, Shinjuku-ku, Tokyo, Japan

[2] Division of General Thoracic Surgery, Department of Surgery, School of Medicine, Keio University, Shinjuku-ku, Tokyo, Japan

ADAM28 (a disintegrin and metalloproteinase 28) is over-expressed in non-small-cell lung cancer (NSCLC) with correlation to cancer cell proliferation, tumor size and lymph node metastasis. The present study was aimed to develop an enzyme-linked immunosorbent assay (ELISA) system for diagnosis and monitoring of NSCLC. Our ELISA specifically measured ADAM28, showing negligible cross-reactivity with other metalloproteinases. The ADAM28 level in the NSCLC tissue was remarkably 36.9-fold higher than that in the non-neoplastic lung tissue ($p < 0.001$). The serum level was significantly 4.6-fold higher in the NSCLC patients (5.41 ± 8.62 ng/ml; $n = 102$) than in the control subjects (1.17 ± 0.93 ng/ml; $n = 20$) ($p < 0.001$), and increased with progress of tumor stage ($p < 0.001$). The level was also significantly higher in the patients with recurrent carcinoma than the control ($p < 0.001$) and in the patients with lymph node metastasis than those without metastasis ($p < 0.001$). The sensitivity, false-negative rate and AUC for ADAM28 were better than those for carcinoembryonic antigen. The combination of both assays improved the sensitivity, specificity, false-positive and false-negative rates for NSCLC. There was a positive correlation between the ADAM28 level measured by ELISA system and the degree of immunostaining in the lung adenocarcinomas with a size of ≤20 mm in diameter. The adenocarcinoma patients showing the high immunohistochemical reaction exhibited a poorer disease-free survival than those with the lower immunoreactivity ($n = 102$; $p < 0.05$). These data demonstrate that our ELISA is specific and sensitive to monitor the levels of ADAM28 in the samples from NSCLC patients and suggest that ADAM28 is a useful serological and histochemical marker for NSCLC.

ADAMs (a disintegrin and metalloproteinases) are a gene family of membrane-anchored proteins that are related to snake venom metalloproteinases and matrix metalloproteinases (MMPs).[1,2] ADAMs consist of prodomain, metalloproteinase, disintegrin, cysteine-rich, epidermal growth factor-like, transmembrane and cytoplasmic tail domains.[1–5] More than 30 genes have been cloned in various species,[1,2] but about one-third of the members are the metalloproteinase-type ADAMs with the zinc-binding consensus motif in their metalloproteinase domains.[2] Although precise biological functions of the metalloproteinase-type ADAMs remain unclear, they may be involved in shedding of membrane proteins, metabolism of growth factors, cell adhesion, cell fusion and cell signaling.[1–5] Accumulated lines of evidence have demonstrated that MMPs play an important role in invasion and metastases of various human cancers mainly through degradation of extracellular matrix.[6–8] Human cancers are also known to express ADAM8, 9, 10, 12, 15, 17, 19 and 28.[2,5,9] We have reported that ADAM28, which consists of 2 isoforms (prototype membrane-anchored form ADAM28m and secreted short form ADAM28s), is over-expressed in human breast cancers and implicated in cancer cell proliferation by promoting the bioavailability of insulin-like growth factor (IGF)-I through digestion of IGF-binding protein 3 (IGFBP-3) in the IGF-I/IGFBP-3 complex.[10] In human lung cancers, ADAM 8, 9, 15, 17 and 28 have been reported to be over-expressed.[11–15] Our previous study showed that ADAM28 is expressed almost selectively by the carcinoma cells in non-small-cell lung cancer (NSCLC) and the expression levels correlate with tumor cell proliferation, tumor size and lymph node metastasis.[14]

Key words: ADAM, lung cancer, biological marker, diagnosis, prognosis

Abbreviations: ADAM: a disintegrin and metalloproteinase; BSA: bovine serum albumin; CEA: carcinoembryonic antigen; CYFRA21-1: cytokeratin 19 fragment; DMEM: Dulbecco's modified Eagle's medium; ELISA: enzyme-linked immunosorbent assay; HRP: horseradish peroxidase; IGF: insulin-like growth factor; IgG: immunoglobulin G; MMP: matrix metalloproteinase; NSCLC: non-small-cell lung cancer; NSE: neuron specific enolase; PBS: phosphate-buffered saline; RT-PCR: reverse transcription-polymerase chain reaction; SCC-Ag: squamous cell carcinoma antigen; SLX: sialyl Lewis^x

Grant sponsor: Ministry of Education, Science and Culture of Japan (Grant-in-Aid for Scientific Research (S)); Grant number: 19109004; Grant sponsor: Ministry of Health and Welfare (Third Term 10-year Strategy for Cancer Control)

DOI: 10.1002/ijc.25212

History: Received 28 May 2009; Accepted 11 Jan 2010; Online 28 Jan 2010

Correspondence to: Yasunori Okada, Department of Pathology, School of Medicine, Keio University, Shinjuku-ku, Tokyo, Japan, Tel.: +81-3-5363-3763, Fax: +81-3-3353-3290, E-mail: okada@sc.itc.keio.ac.jp

Lung cancer is one of the most common cancers and a major cause of mortality in many industrialized countries.[16] NSCLC represents about 80% of all lung cancers,[17] and surgical resection (lobectomy and pneumonectomy with lymph node sampling or dissection) remains the mainstay of therapy for NSCLC patients, offering the best chance of cure. However, the majority of the diagnosed patients with NSCLC are in an advanced stage and they are not candidates for surgical interventions and radiation therapy. Although the chemotherapy may extend the survival of the advanced lung cancer patients and relax a symptom, the prognosis still remains poor.[18–20] Thus, early detection contributes to improve the survival. In addition, the postoperative 5-year survival of NSCLC patients of Stage I does not reach 80% mainly because of carcinoma recurrence.[21,22] These indicate the importance of the markers for diagnosis and monitoring cancer recurrence. Carcinoembryonic antigen (CEA), squamous cell carcinoma antigen (SCC-Ag), neuron specific enolase (NSE), cytokeratin19 fragment (CYFRA21-1) and sialyl Lewis^x (SLX) have been commonly used as tumor markers for NSCLC,[23–29] but none of these markers appear to be sufficiently sensitive and specific to be reliable for screening and diagnosis of NSCLC, especially early-stage lung cancers.[25–27] If one marker could discriminate between patients with or without lung cancer, it might be suitable for screening of diagnosis and would contribute to improvement of mortality rate.

In the present study, we established an enzyme-linked immunosorbent assay (ELISA) system for ADAM28 using 2 mouse monoclonal antibodies. We applied this system to the samples of human carcinoma cell lines, lung carcinoma tissues, serum and urine. The serum levels of ADAM28 in the NSCLC patients were compared with those in the control normal subjects and among the patient groups classified according to the clinicopathological parameters. ADAM28 was also detectable by immunoblotting and measurable by the ELISA system in the urine samples from the patients. The disease-free survival and overall survival rates were calculated based on the immunohistochemical results in the patients with adenocarcinoma of $\leq$20 mm in diameter. Our study provides the first evidence that ADAM28 may be a useful serological and/or histochemical marker for NSCLC.

Material and Methods

Preparation of mouse monoclonal antibodies against ADAM28

Monoclonal antibodies against ADAM28 were developed by using purified recombinant proADAM28s (a precursor of ADAM28s) as an antigen according to our previous methods.[14,30,31] Six clones (297-2F3, 297-1E3, 297-1A5, 297-3B10, 297-3B6 and 297-3D10) secreting immunoglobulin G (IgG) were selected after screening by ELISA system using recombinant ADAM28s.[14] Monospecificity of the clones was determined by immunoblotting of the culture media containing proADAM28s as described previously.[14] All these antibodies specifically recognized proADAM28s, and clones 297-2F3 and 297-1E3, both of which were used for the ELISA system (see below), were reactive with the metalloproteinase domain of ADAM28[14] (data not shown for 297-1E3).

Development of ELISA system for ADAM28

The 6 monoclonal anti-ADAM28 antibodies were conjugated with horseradish peroxidase (HRP) according to the methods previously described.[32] Briefly, HRP in distilled water was reacted with 0.1 mM sodium periodate for 20 min at 23°C and then dialyzed against 1 mM sodium acetate, pH 4.0 at 4°C overnight. Equal volume (100 μl) of 5 mg/ml monoclonal antibody and 4 mg/ml activated HRP, pH of which had been adjusted to 9.0–9.5 with 0.2 M sodium carbonate, was incubated for 2 hr at 37°C. After stopping the reaction by incubation with 4 mg/ml sodium tetrahydroborate, the mixture was dialyzed against phosphate-buffered saline, pH 7.0 (PBS) at 4°C overnight.

Microtiter plates with 96 wells (Nalge Nunc International, Rochester, NY) were coated with 100 μl of 1 μg/ml nonlabeled antibody in PBS at 4°C overnight and then incubated with 1% bovine serum albumin (BSA) for 1 hr. After washing with PBS 7 times, 50 μl enzyme solutions containing different concentrations of ADAM28 were added to the plates and incubated for 2 hr at 23°C. After washing with PBS, the plates were incubated with 2.5 μg/ml HRP-conjugated antibody in 1% BSA for 1 hr at 23°C, washed with PBS and then reacted with 1 mg/ml *O*-phenylenediamine and 0.02% hydrogen peroxide in 100 mM citric acid buffer, pH 6.0 for 30 min. The reaction was stopped with 4 N sulfuric acid and the absorbance at 492 nm was measured by a microplate reader (Powerscan-HT, DS Pharma Biomedical Co., Osaka, Japan). Cross-reactivity with other ADAMs and MMPs was examined by using authentic proteins including ADAM8 (R&D System, Minneapolis, MN), ADAM9 (R&D System), ADAM10 (R&D System), ADAM12,[33] ADAM17 (R&D System), ADAMTS1 (R&D System), ADAMTS4,[34] ADAMTS5 (R&D System), proMMP-1 (Calbiochem, La Jolla, CA), proMMP-2,[35] proMMP-3,[36] proMMP-7,[37] proMMP-9[38] and proMMP-13 (Calbiochem). All the ADAM and proMMP species were diluted with PBS and incubated in the microtiter plates. After the reactions, the absorbance was measured with the PBS-incubated samples as a control.

Immunoblotting of ADAM28 and application of the ELISA system to carcinoma cell lines and lung tissues

Cancer cell lines established from lung squamous cell carcinoma (SK-MES-1), lung adenocarcinoma (Lu-1, PC9, A549 and H1650), pancreatic adenocarcinoma (PANC1) and breast carcinoma (MCF-7) were maintained in RPMI-1640 containing 10% heat-inactivated fetal bovine serum and antibiotics in a humidified atmosphere of 5% CO_2 at 37°C. The subconfluent cells were cultured in serum-free RPMI-1640 medium for 2 days and the culture media were harvested. Cell lysates were prepared in 50 mM Tris-HCl buffer, pH 7.5, 150 mM NaCl, 10 mM $CaCl_2$ and 0.01% Brij 35 (TNCB buffer)

containing a cocktail of proteinase inhibitors (Complete Mini, Roche Diagnostics, Mannheim, Germany) and concentrations of the supernatants of cell lysates were measured by Proteostain (Dojindo, Kumamoto, Japan) using BSA as a standard. Both cell lysates (100 μg/well) and concentrated culture media (1 ml of the original media/well) were subjected to the ELISA for ADAM28. Concentrations of ADAM28 in the cell lysates and culture media were calculated by dividing the amounts of ADAM28 protein in the lysates and media by total proteins of the cell lysates. Proteins in the homogenate supernatants were also analyzed by immunoblotting. The homogenate samples (20 μg/lane) were subjected to sodium dodecyl sulfate-polyacrylamide gel electrophoresis (SDS-PAGE) under reducing conditions and transferred onto polyvinylidene difluoride membranes. The membranes were blotted with anti-ADAM28 antibody specific to the metalloproteinase domain of ADAM28 (5 μg/ml; 297-2F3), anti-ADAM28 antibody specific to the cytoplasmic domain of ADAM28m (1 μg/ml, CL1ADAM28; Cedarlane Labs, Hornby, Ontario, Canada) or anti-β-actin antibody (0.2 μg/ml; Sigma-Aldrich, St. Louis, MO) after blocking nonspecific reactions. As for a control, they were reacted with nonimmune mouse IgG (5 μg/ml; Sigma-Aldrich) or rabbit IgG (1 μg/ml; DAKO, Glostrup, Denmark). The membranes were then incubated with secondary antibody (1:5,000; Amersham Pharmacia Biotech, Buckinghamshire, UK) and immunoreactive protein bands were detected with ECL immunoblotting reagents (Amersham Pharmacia Biotech).

Lung carcinoma tissue samples consisted of adenocarcinomas ($n = 6$) and squamous cell carcinomas ($n = 6$) and their non-neoplastic lung tissues ($n = 12$) distant from the cancers in the same lobes were snap-frozen in liquid nitrogen immediately after surgically removed and stored at −80°C. The carcinoma and non-neoplastic lung tissues were homogenized on ice in TNCB buffer containing a cocktail of proteinase inhibitors. Supernatants of the tissue homogenates (20 μg/well) were subjected to ELISA.

Preparation of serum samples from the patients with NSCLC or normal healthy subjects for ELISA

Serum samples were obtained at the time of pathological or cytological diagnosis from a total of 102 patients (90 patients with primary NSCLC and 12 patients with recurrent NSCLC) (71 males and 31 females) ranging from 36 to 84 years of age (66 ± 11 years old; mean ± SD), who were admitted to the Keio University Hospital, Tokyo, Japan. The control group consisted of 20 healthy volunteers (10 males and 10 females) ranging from 45 to 83 years of age (68 ± 9 years old). The 102 NSCLC cases consisted of adenocarcinoma (67 cases), squamous cell carcinoma (21 cases), NSCLC, in which specific histopathological diagnosis could not be made because of limited amount of the biopsied tissue samples (8 cases), pleomorphic carcinoma (3 cases), large cell carcinoma (2 cases) and adenosquamous carcinoma (1 case). Histological typing of the tumors was carried out according to the WHO classification,[39] and pathological stages were determined by the current TNM classification.[40] None of the patients except for those with recurrent carcinoma had been treated by chemotherapy or irradiation. The clinical data for staging were obtained by computed tomography scan of the chest and abdomen, magnetic resonance imaging of the head, abdominal echo, bone scintigraphy and/or positron emission tomography. Serum samples were stored at −80°C before used for ELISA of ADAM28 and CEA, the latter of which was commercially available electrochemiluminescence immunoassay (Roche Diagnostics, Tokyo, Japan). Informed consent was obtained from the patients and normal subjects according to the hospital ethical guidelines. The profiles of the patients with primary NSCLC ($n = 90$) are summarized in Table 1.

Preparation of urine samples from the NSCLC patients or normal healthy subjects for immunoblotting and ELISA

Urine samples were collected from 91 patients with NSCLC (61 males and 30 females) aged ranging from 41 to 84 years old (66 ± 10 years old). The 91 NSCLC cases consisted of adenocarcinoma (58 cases), squamous cell carcinoma (19 cases), NSCLC diagnosed without specific histopathological diagnosis because of the tissue limitation (9 cases), pleomorphic carcinoma (2 cases), large cell carcinoma (2 cases) and adenosquamous carcinoma (1 case). None of the patients had been treated by chemotherapy or irradiation. The control group consisted of 20 healthy volunteers (13 males and 7 females) aged from 50 to 70 years old (62 ± 7 years old). Informed consent was obtained from the patients and normal subjects according to the hospital ethical guidelines.

The morning midstream voided urine samples (10–20 ml) were collected and tested by Multistix 9 urinalysis strips (Bayer, Ellhart, IN), and the positive samples containing red blood cells and/or leukocytes were excluded from the experiments. The samples were subjected to centrifugation at 4,000*g* for 15 min at 4°C to remove insoluble materials. The 10-ml urine samples were concentrated by centricon (Millipore, Billerica, MA) and then proteins were precipitated with 3.3% trichloroacetic acid. After centrifugation, the pellets were subjected to immunoblotting for ADAM28 as described above. Since more than half numbers of the urine samples ($n = 55$) were used up for immunoblotting, the remaining samples from lung carcinoma patients ($n = 26$) and control subjects ($n = 10$) were also subjected to ELISA for ADAM28.

Immunohistochemistry for ADAM28 in the lung adenocarcinomas

Carcinoma tissues ($n = 102$) obtained from the patients with adenocarcinoma of ≤20 mm in diameter, whose clinical courses were monitored for 7 years, were fixed with buffered formalin and paraffin sections (4-μm thick) were made. After dewaxed, the sections were treated with 0.3% hydrogen peroxide in methanol and 10% normal goat serum to block endogenous peroxidase and nonspecific binding, respectively.

Table 1. Characteristics of the patients with primary NSCLC

Variable		No. of patients (n = 90)	ADAM28 (ng/ml) (Mean ± SD)	p value*
Age (years)	<70	49	5.78 ± 9.26	0.563
	≥70	41	4.96 ± 7.64	
Gender	Male	62	6.10 ± 9.94	0.104
	Female	28	3.79 ± 4.04	
Tumor size (mm)	<30	59	4.17 ± 7.27	<0.001
	≥30	31	6.97 ± 9.89	
Histology	ADC	57	5.45 ± 8.80	0.859
	SCC	20	3.90 ± 3.71	
	Others	13	3.78 ± 1.77	
Stage	I	50	2.36 ± 1.90	<0.001
	II + III + IV	40	9.16 ± 11.7	
T factor	T1	50	4.14 ± 7.29	<0.001
	T2	29	4.96 ± 4.88	
	T3 + T4	11	12.0 ± 15.8	

*Mann–Whitney U test.Abbreviations: ADC, adenocarcinoma; SCC, squamous cell carcinoma.

Then, they were reacted with anti-ADAM28 antibody (10 μg/ml; 297-2F3) at 4°C overnight and incubated with biotinylated anti-mouse IgG (1/200 dilution; Vector Laboratories, Burlingame, CA). Immunostaining was performed by the peroxidase-labeled avidin-biotin-complex method (1/100 dilution; DAKO).[10,14] As a control, sections were reacted by replacing the primary antibody with nonimmune mouse IgG (10 μg/ml; DAKO). After the reactions, the sections were counterstained with hematoxylin. Grading of immunostaining (% of immunostained carcinoma cells to total carcinoma cells) was carried out without any knowledge of the clinical data according to our methods as described previously.[10,14] Since frozen adenocarcinoma tissues were available with 37 cases, tissue homogenates were prepared from the samples and the supernatants were subjected to ELISA for ADAM28. The data of ELISA were compared with the immunostaining grade. To examine whether ADAM28m and/or ADAM28s are produced in these adenocarcinoma samples, the homogenates (70 μg/lane) were analyzed by immunoblotting with anti-ADAM28 antibodies specific to the ADAM28 metalloproteinase domain (297-2F3) or the ADAM28m cytoplasmic domain (CL1ADAM28; Cedarlane Labs) or anti-β-actin antibody (Sigma-Aldrich) as described above.

Statistical analyses

All of the data were analyzed with SPSS software (SPSS version 15.0J). Sensitivity, specificity, false-positive and false-negative rates and likelihood ratio were compared using standard formulas. Differences in the levels of ADAM28 and CEA and comparison between the immunoblotting data of ADAM28 in the urine samples from cancer groups and controls were analyzed by Mann–Whitney U tests. Comparison among more than 3 groups was determined by the Kruskal–Wallis test. The correlation for 2 markers was analyzed by the Pearson's correlation coefficient. Analysis of survival was performed using the method of Kaplan–Meier, and comparison of survival between patient groups was done by Log-rank test. P values less than 0.05 were considered significant.

Results

Development of ELISA system for ADAM28

Using 6 monoclonal antibodies against ADAM28 (297-2F3, 297-1E3, 297-1A5, 297-3B10, 297-3B6 and 297-3D10), we tried to develop the ELISA system for ADAM28 by testing total 30 combinations of the 2 monoclonal antibodies. As a result, the combination of 297-1E3 (the solid phase) and 297-2F3 (the conjugate coupled with HRP) was found to be the most sensitive for detection of recombinant ADAM28. When the cross-reactivity of the antibodies in the ELISA system was examined against ADAM8, ADAM9, ADAM10, ADAM12, ADAM17, ADAMTS1, ADAMTS4, ADAMTS5, proMMP-1, proMMP-2, proMMP-3, proMMP-7, proMMP-9 and proMMP-13, negligible reaction with these ADAMs, ADAMTSs or proMMPs was obtained (Table 2).

Standard assay curve for ADAM28 by the ELISA system and its validation

The sensitivity of the assay for standard recombinant ADAM28 was 0.1 ng/ml, which was calculated as the concentration that is 2 standard deviations above the zero standard. Linearity was obtained between 0.1 and 10.0 ng/ml (Fig. 1). The values of intra-assay coefficient of variation (C.V.), which represents [standard deviation/mean] × 100, of normal serum containing ADAM28 at concentrations of 1.25, 2.5 and 5.0 ng/ml were 2.5–4.6% (n = 5). Interassay C.V.

Table 2. Cross-reactivity of the ELISA system for ADAM28 with other ADAMs, ADAMTSs and proMMPs

	Concentration (ng/ml)	A492
ADAM28	1	0.241 ± 0.003
	5	1.825 ± 0.031
ADAM8	5	0.038 ± 0.001
ADAM9	5	0.027 ± 0.001
ADAM10	5	0.015 ± 0.002
ADAM12	5	0.067 ± 0.002
ADAM17	5	0.019 ± 0.001
ADAMTS1	5	0.033 ± 0.001
ADAMTS4	5	0.054 ± 0.001
ADAMTS5	5	0.064 ± 0.001
ProMMP-1	5	0.070 ± 0.002
ProMMP-2	5	0.092 ± 0.001
ProMMP-3	5	0.085 ± 0.001
ProMMP-7	5	0.090 ± 0.001
ProMMP-9	5	0.091 ± 0.002
ProMMP-13	5	0.005 ± 0.001

The assay was triplicated and the data are presented as mean ± SD.

values were 4.3–6.2% (n = 5) at serum ADAM28 levels of 1.25, 2.5 and 5.0 ng/ml. Recoveries of standard ADAM28 added to human serum containing ADAM28 at a concentration of 5 ng/ml over range of 0.1–5.0 ng/ml were (103.9 ± 10.8)% (mean ± SD.).

Measurement of ADAM28 in cancer cell lines and NSCLC tissues

By immunoblotting, cell lysates of all 5 lung carcinoma cell lines (SK-MES-1, Lu-1, PC9, A549 and H1650) showed several major immunoreactive bands including 65-, 55/57-, 42- and 27-kDa bands with anti-ADAM28 antibody specific to the metalloproteinase domain (297-2F3), whereas no definite immunoreactive bands were observed in PANC1 and MCF-7 cell lysates (Fig. 2*a*). Among them, the 55/57-kDa bands were immunoreactive with anti-ADAM28 antibody specific to the cytoplasmic domain of ADAM28m (Fig. 2*a*), indicating that they represent active forms of ADAM28m as we previously reported.[10] According to the molecular weight of the immunoreactive bands and their negative immunoreactivity to the antibody against ADAM28m, the 65-kDa and 42-kDa bands are considered to be proADAM28s and active ADAM28s, respectively[10,14,31] and the 27-kDa band may be a degraded form containing the metalloproteinase domain of ADAM28. In accord with the immunoblotting data, ADAM28 was measurable in these carcinoma cell lysates by the ELISA system, but it was negligible in the samples of PANC1 and MCF-7 cell lines (Fig. 2*a*). The immunoblotting patterns appeared to be similar to the ADAM28 levels measured by the ELISA system (Fig. 2*a*). Lower levels of

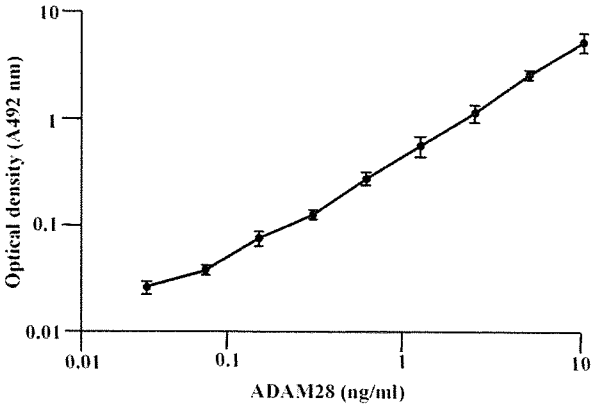

Figure 1. Standard curve by the ELISA system for ADAM28. Purified proADAM28 was determined by the ELISA system consisting of 2 monoclonal antibodies (297-1E3 as a solid phase and 297-2F3 as HRP-conjugate) using microtiter plates as described in Material and Methods.

ADAM28 were also detectable by the ELISA system in the culture media from the lung carcinoma cell lines, but the level was negligible in those from PANC1 and MCF-7 cell lines (Fig. 2*b*). We also measured the levels of ADAM28 in homogenates of the NSCLC tissues and their non-neoplastic lung tissues by our ELISA system. As shown in Figure 2*c*, the level was remarkably 36.9-fold higher in the carcinoma tissues (53.2 ± 17.2 ng/mg protein) than in the non-neoplastic tissues (1.4 ± 0.4 ng/mg protein) ($p < 0.001$; n = 12 each).

Serum levels of ADAM28 in the patients with NSCLC and their correlations with clinicopathological parameters

The serum samples from the patients with NSCLC and control healthy subjects were subjected to our ELISA system. The mean level of ADAM28 in the carcinoma patients (n = 102) was 5.41 ± 8.62 ng/ml (data not shown), which was significantly 4.6-fold higher than in the controls (1.17 ± 0.93 ng/ml; n = 20) ($p < 0.001$) (Fig. 3*a*). When the level was compared among the tumor stages, it was gradually and significantly increased with progress of the stage ($p < 0.001$) (Fig. 3*a*). The level of ADAM28 was significantly 2.0-fold higher in Stage I (2.36 ± 1.90 ng/ml; n = 50) than in the controls ($p < 0.01$) and it was also significantly 2.1-fold higher in Stage II (5.05 ± 1.56 ng/ml; n = 12) than in Stage I ($p < 0.001$). The levels in Stage III (9.76 ± 1.1.72 ng/ml; n = 17) and Stage IV (12.71 ± 15.80 ng/ml; n = 11) were not significantly different from those in Stage I or Stage II (Fig. 3*a*), but the level in Stages II–IV (9.16 ± 11.7 ng/ml; n = 40) was significantly higher than that in Stage I ($p < 0.001$) (Table 1). Importantly, the patients with recurrent carcinoma showed a significantly higher level of ADAM28 (9.93 ± 8.56 ng/ml; n = 12) than the control subjects ($p < 0.001$) (Fig. 3*a*). In addition, the level in the patient group with lymph node metastasis (9.78 ± 12.5 ng/ml; n = 35) was

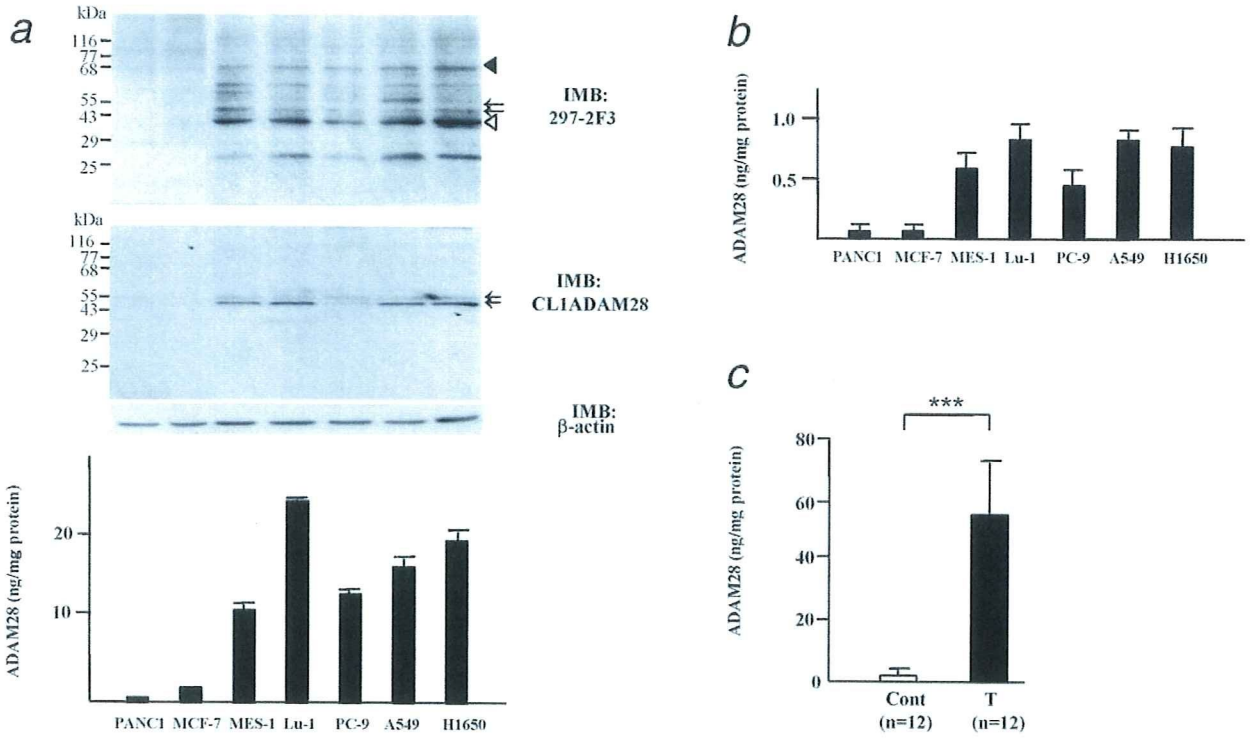

Figure 2. The expression of ADAM28 species in cell lysates and culture media of human cancer cell lines and homogenates of human NSCLC and non-neoplastic lung tissues. (*a*) Immunoblotting and ELISA analyses of ADAM28 in the cell lysates of cancer cell lines. Cell lysates from lung squamous cell carcinoma (SK-MES-1), lung adenocarcinoma (Lu-1, PC9, A549 and H1650), pancreatic adenocarcinoma (PANC1) and breast carcinoma (MCF-7) were subjected to immunoblotting (IMB) using anti-ADAM28 antibodies specific to the metalloproteinase domain of ADAM28 (297-2F3; upper panel) or the cytoplasmic domain of ADAM28m (CL1ADAM28; middle panel) as described in Material and Methods. Closed arrowhead, arrows and open arrowhead, 65-kDa proADAM28s, 55/57-kDa active ADAM28m and 42-kDa active ADAM28s, respectively. The samples were also applied to the ELISA system for ADAM28 (lower panel). MES-1, SK-MES-1. (*b*) ELISA analyses of ADAM28 in the culture media of cancer cell lines. Culture media from the cell lines were subjected to the ELISA system. (*c*) Analysis of ADAM28 production levels in NSCLC (T) and control non-neoplastic tissues (Cont) by the ELISA system. ***, $p < 0.001$.

significantly 3.8-fold higher than that in the group without metastasis (2.58 ± 1.99 ng/ml; $n = 55$) ($p < 0.001$) (Fig. 3*b*). It was also significantly increased with the tumor size ($p < 0.001$) (Fig. 3*c*) and the T factor (Table 1).

Comparison of ADAM28 and CEA as tumor markers

Since CEA in serum samples is used as a prevalent maker for diagnosis and monitoring of NSCLC, we compared the sensitivity, specificity and false-positive and false-negative rates of ADAM28 with those of CEA. When the cutoff level of ADAM28 assay was set as 1.72 ng/ml according to the value of mean ± 2SD of the healthy controls, the sensitivity, specificity, false-positive and false-negative rates of ADAM28 in the NSCLC samples were 72.5, 76.5, 23.5 and 27.5%, respectively (Table 3). On the other hand, those of the CEA assay with the upper limit of normal defined as 5.60 ng/ml in our hospital were 30.6, 88.2, 11.8 and 69.4%, respectively (Table 3). The specificity and false-positive rate with a 3.20 ng/ml cutoff of ADAM28 assay were improved to 100 and 0%, respectively, but the sensitivity and false-negative rate were worse than those with a 1.72 ng/ml cutoff (Table 3). The mean area under the receiver-operating characteristic curve (AUC) for ADAM28 was 0.79 (95% confidence interval = 0.76–0.86), whereas AUC for CEA was 0.56 (95% confidence interval = 0.44–0.67) (Fig. 4*a*). In accord with the fact that the 2 tumor markers are different in character (a metalloproteinase *versus* a carbohydrate chain antigen of colon origin), there was no significant correlation between the serum levels of ADAM28 and CEA ($r = 0.158$, $p = 0.149$; $n = 90$) (Fig. 4*b*). Therefore, when the 2 markers were applied to the samples, the sensitivity, specificity, false-positive and false-negative rates were improved up to 81.2, 94.1, 5.9 and 18.8%, respectively (Table 3).

ADAM28 in human urine samples from NSCLC patients

To examine whether ADAM28 is secreted into urine, we performed immunoblotting for ADAM28 in the urine samples from patients with NSCLC and control subjects. As shown in Figure 5*a*, immunoblotting demonstrated an ADAM28 protein band of 42 kDa in 37.4% of the samples from the

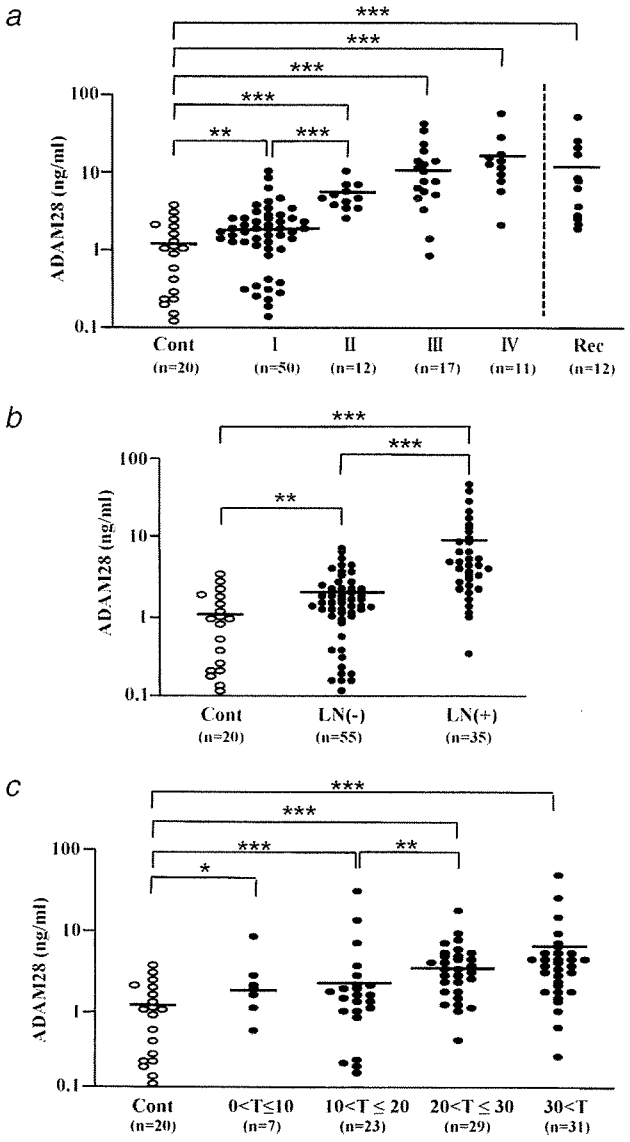

Figure 3. Comparison of serum concentrations of ADAM28 in patients with NSCLC and control healthy subjects. Serum ADAM28 was measured by the ELISA system in serum samples from the NSCLC patients and control subjects. (*a*) Serum concentrations of ADAM28 in control subjects (Cont) or patients with primary NSCLC at Stages I–IV or recurrent NSCLC (Rec). (*b*) Serum levels of ADAM28 in control subjects (Cont) or patients with or without lymph node metastasis. LN(−), patients without lymph node metastasis; LN(+), patients with lymph node metastasis. (*c*) Serum levels of ADAM28 in control subjects (Cont) or NSCLC patients with tumor sizes of 0 mm $< T \leq$ 10 mm, 10 mm $< T \leq$ 20 mm, 20 mm $< T \leq$ 30 mm or 30 mm $< T$. *, $p < 0.05$; **, $p < 0.01$; ***, $p < 0.001$.

Table 3. Characteristics of serum ADAM28 and CEA

	ADAM28		CEA	ADAM28 + CEA
Cutoff level (ng/ml)	1.72	3.20	5.60	1.72/5.60
Sensitivity (%)	72.5	47.3	30.6	81.2
Specificity (%)	76.5	100	88.2	94.1
False-positive rate (%)	23.5	0	11.8	5.9
False-negative rate (%)	27.5	52.7	69.4	18.8
Positive likelihood ratio	3.1	–	2.6	11.8
Negative likelihood ratio	0.4	0.5	0.8	0.2

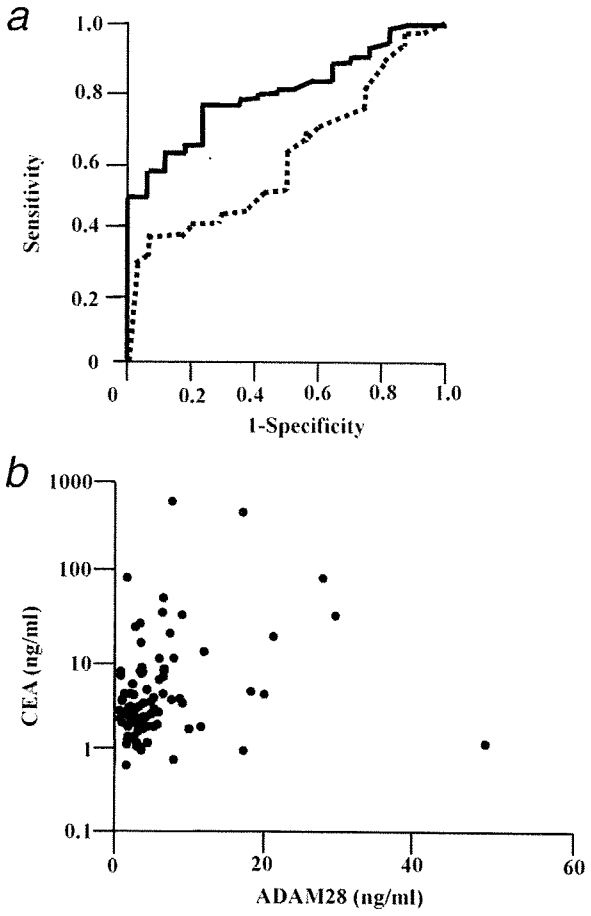

Figure 4. Receiver-operating characteristic curves for ADAM28 and CEA, and correlation between concentrations of ADAM28 and CEA in NSCLC patients. (*a*) Serum concentrations of ADAM28 and CEA in NSCLC samples ($n = 90$) and control samples ($n = 20$) were determined by the ELISA systems. Receiver-operating characteristic curves for ADAM28 (solid line) and CEA (dotted line) were derived by plotting the relationship between the specificity and the sensitivity at various cutoff levels. (*b*) Correlation between serum concentrations of ADAM28 and CEA in NSCLC patients ($n = 90$).

carcinoma patients (34/91 samples), but none of the samples from the healthy controls (0/20 samples) showed the immunoreactive band. The detection rate of ADAM28 was significantly higher in the cancer patients than in the controls ($p < 0.001$), and gradually increased with progress of the stage ($p < 0.001$) (Fig. 5*b*). When concentrations of ADAM28 in the urine and serum samples from the cancer patients ($n = 26$) and controls ($n = 10$) were compared, there was a direct

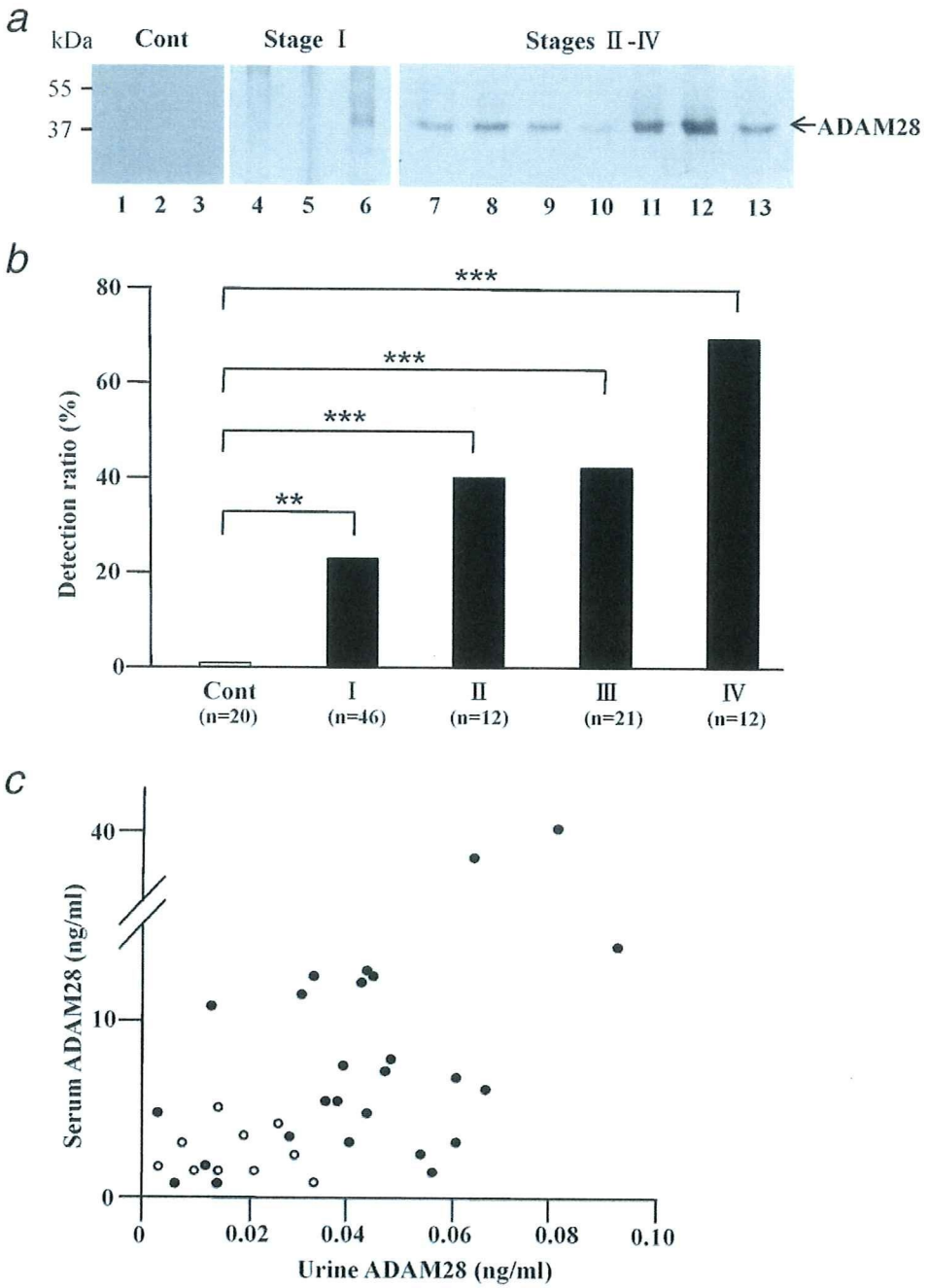

Figure 5. Immunoblotting and ELISA analyses of ADAM28 in urine samples from NSCLC patients or control normal subjects, and correlation between the levels of ADAM28 in serum and urine samples. (*a*) Immunoblotting of ADAM28 in urine samples. Urine samples from control subjects (Cont) and NSCLC patients (Stage I and Stages II–IV) were subjected to immunoblotting with anti-ADAM28 antibody specific to the metalloproteinase domain (297-2F3) as described in Material and Methods. The arrow indicates the 42-kDa band of ADAM28. The 13 representative samples are shown. Lanes 1–3, control samples; Lanes 4–6, Stage I NSCLC samples; Lanes 7–13, Stages II–IV NSCLC samples. (*b*) Detection rate of the ADAM28 protein band by immunoblotting in urine samples from control subjects and NSCLC patients at clinical Stages I, II, III and IV. **, $p < 0.01$; ***, $p < 0.001$. (*c*) Correlation between the serum and urine levels of ADAM28 measured by the ELISA system ($r = 0.474$, $p < 0.01$; $n = 36$). ○, control subjects; •, NSCLC patients.

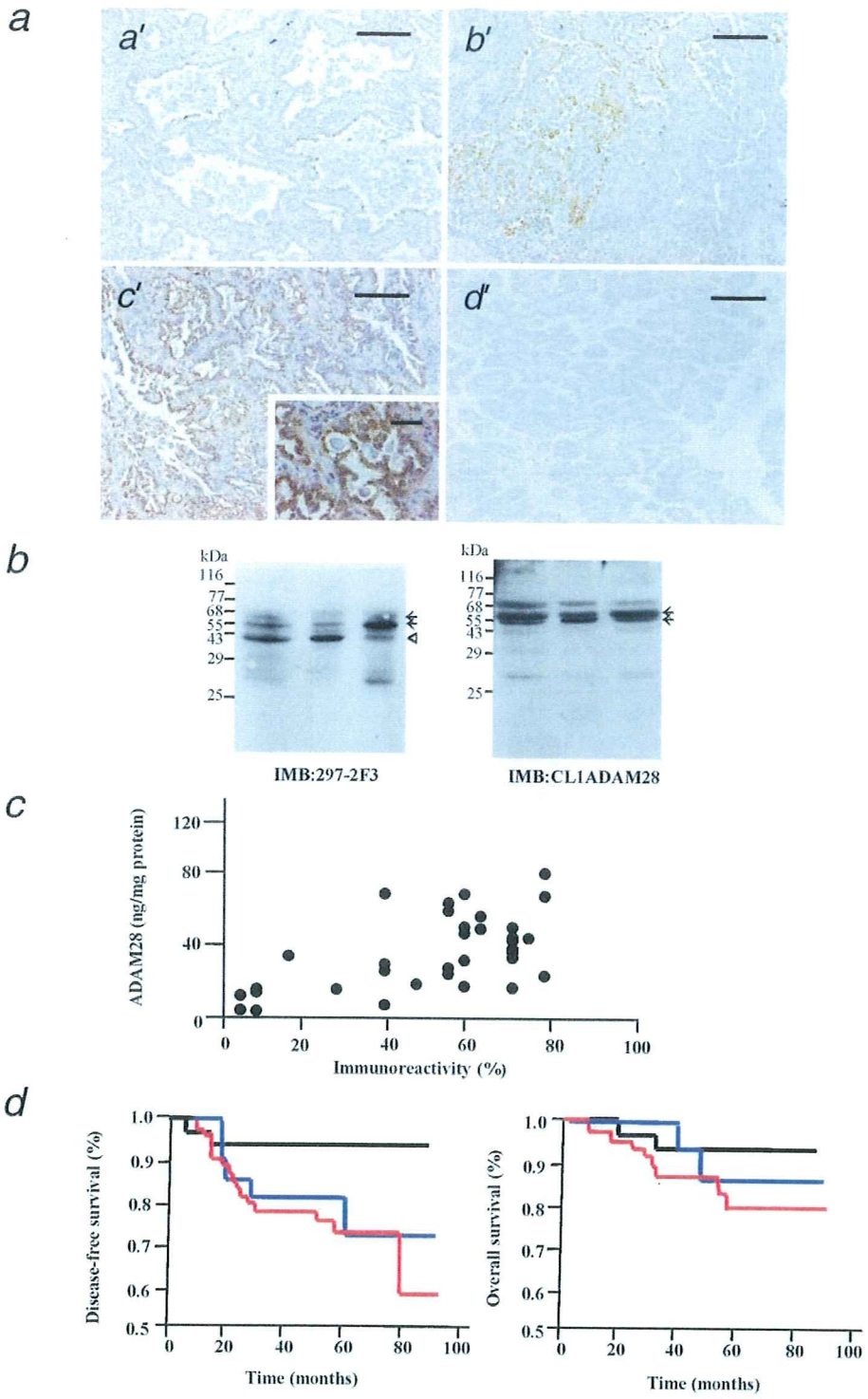

Figure 6. Immunostaining of ADAM28 and its correlation with ADAM28 production levels in adenocarcinomas with a tumor size of ≤20 mm in diameter, immunoblotting of ADAM28 in the adenocarcinoma tissues and Kaplan–Meier graphs of disease-free survival and overall survival. (*a*) Immunostaining of ADAM28 in adenocarcinoma with anti-ADAM28 antibody to the metalloproteinase domain (297-2F3) (A–C) or nonimmune mouse IgG (D). A, B, C and D: adenocarcinomas obtained from patients in Stage I (A), II (B) or III (C and D). Note that immunostaining is predominantly observed in the carcinoma cells, showing more immunoreactive cells with staging. Inset, high-power view of the carcinoma cells. Scale bars, 50 μm. (*b*) Immunoblotting (IMB) of ADAM28 in the adenocarcinoma tissues with anti-ADAM28 antibody (297-2F3) and anti-ADAM28 antibody specific to the cytoplasmic domain of ADAM28m (CL1ADAM28). Samples are from the patients of Stages III, II and III from the left. Arrows and open arrowhead, 55/57-kDa ADAM28m and 42-kDa ADAM28s. (*c*) Correlation between the immunoreactivity and the ADAM28 level in the carcinoma tissues ($r = 0.539$, $p < 0.01$; $n = 37$). (*d*) Kaplan–Meier graphs of disease-free survival (left) and overall survival (right). Black line, the low-expressing group ($n = 32$); blue line, the medium-expressing group ($n = 20$); red line, high-expressing group ($n = 50$).

correlation between the levels of ADAM28 in the urine and the serum samples ($r = 0.474$, $p < 0.01$; $n = 36$) (Fig. 5*c*). A similar direct correlation was also observed with the urine and serum samples from the cancer patients alone ($r = 0.600$, $p < 0.01$; $n = 26$) (data not shown).

Immunohistochemistry of ADAM28 as a prognostic marker for the patients with lung adenocarcinoma

Although our previous study showed that ADAM28 is immunolocalized to the carcinoma cells of the lung adenocarcinomas, the study did not clarify the relationship between the degree of the immunostaining and the production level in the carcinoma tissues.[14] Thus, we compared the level of ADAM28 measured by the ELISA system and the degree of immunostaining in the carcinoma cells using the adenocarcinomas with a tumor size of ≤20 mm in diameter, the clinical courses of which were monitored for 7 years. Stages of the adenocarcinoma patients ($n = 102$) included Stages I (91 cases), II (3 cases) and III (8 cases). The level of ADAM28 protein in the adenocarcinoma tissues ($n = 37$) was 61.8 ± 35.0 ng/mg protein, ranging from 5.87 to 110.30 ng/mg protein. By immunohistochemistry, ADAM28 was localized predominantly to the carcinoma cells in all the carcinoma samples examined (Fig. 6*a*) and the proportion of ADAM28-immunostained carcinoma cells to total carcinoma cells (immunoreactivity) was (64.9 ± 33.9)%, ranging from 5 to 100%. Immunoreactivity appears to increase with staging of the adenocarcinoma patients, and negligible or no staining was observed with nonimmune IgG (Fig. 6*a*). Immunoblotting analyses for ADAM28 of the carcinoma tissues showed that all the samples examined ($n = 31$) contain active forms of 42-kDa ADAM28s and 55/57-kDa ADAM28m forms (Fig. 6*b* for representative 3 cases and data not shown for others), although the immunoblotting patterns of the molecular species or the density of the immunoreactive bands showed no definite correlation with the stages of the patients. When the ADAM28 level and the ADAM28 immunoreactivity were compared in each case, there was a significant correlation between the 2 groups ($r = 0.539$, $p < 0.01$; $n = 37$) (Fig. 6*c*), suggesting that the immunostaining reflects the production levels by the carcinoma cells. To study the relationship between the immunohistochemical ADAM28 expression and the disease-free survival after operation and overall survival, a larger number of the carcinoma cases ($n = 102$) were analyzed by classifying them to the low-expressing group (immunoreactivity ≤ 1–49%) (20.6% ± 15.4%; $n = 32$), medium-expressing group (immunoreactivity ≤ 50–79%) (63.0% ± 9.7%; $n = 20$) and high-expressing group (immunoreactivity ≥ 80%) (94.0% ± 6.1%; $n = 50$). As shown in Figure 6*d*, disease-free survival after operation was significantly lower in the high-expressing group than in the low-expressing and medium-expressing groups, although a significant difference was not obtained ($p = 0.073$) (Fig. 6*d*).

Discussion

In the present study we have established an ELISA system for human ADAM28 using a combination of 2 monoclonal antibodies against ADAM28. The ELISA system was specific to ADAM28, since only negligible reaction was observed with ADAM8, 9, 10, 12 and 17, ADAMTS1, 4 and 5 and proMMP-1, 2, 3, 7, 9 and 13, all of which are members of the metalloproteinase gene families. The 2 antibodies used for the ELISA system were reacted with the metalloproteinase domain of ADAM28, and the immunoblotting patterns of ADAM28 species in cell lysates appeared similar to the levels measured by the ELISA system. Therefore, the assay is expected to detect all the ADAM28 species within the samples, that is, both precursor and active forms of ADAM28s and ADAM28m, and is considered to be suitable to measure a total amount of ADAM28 species in the clinical samples. In fact, the ADAM28 levels were remarkably high in the NSCLC tissues and negligible in the non-neoplastic lung tissue, confirming our previous immunohistochemical data of ADAM28.[14]

Our study has demonstrated that the serum levels of ADAM28 are significantly higher in the NSCLC patients than in the control normal subjects, and that the level gradually increases with the staging of NSCLC. Importantly, the level is significantly higher even in the Stage I patients than in the control subjects, suggesting that this assay system is applicable to screening of NSCLC patients at early stages. There was a positive correlation between the ADAM28 level and the tumor size, and the level was significantly higher in the patients with recurrent tumors than in the control subjects. We have previously reported that the mRNA expression levels of ADAM28 correlate with MIB1-positive cell index (a marker of cell proliferation) and lymph node metastasis in NSCLC patients.[14] Thus, the data in the current study are accordant to our previous findings on the clinicopathological correlations. The present immunoblotting study showed that active forms of both ADAM28s and ADAM28m are present in the adenocarcinoma tissues. Therefore, it seems plausible that ADAM28s secreted by NSCLC cells is drained into blood. However, our study does not completely exclude the possibility that ADAM28 detected in the serum samples may contain ADAM28m shed from NSCLC cells in addition to ADAM28s, although no data on the shedding of ADAM28m have been provided.

Previous study showed that ADAM28 is over-expressed, probably by stellate cells, in biopsied liver tissues from patients with chronic liver diseases and the expression levels correlate with degree of liver fibrosis.[41] This raises questions of whether ADAM28 is over-expressed in the lung tissues from patients with fibrotic and/or chronic inflammatory lung diseases such as interstitial pneumonia, chronic obstructive lung disease and bronchial asthma, and whether the serum